PHYSICAL REVIEW B **88**, 205303 (2013)

Wigner function approach to single electron coherence in quantum Hall edge channels

D. Ferraro, A. Feller, A. Ghibaudo, and E. Thibierge
Université de Lyon, Fédération de Physique André Marie Ampère, CNRS, Laboratoire de Physique de l'Ecole Normale Supérieure de Lyon, 46 Allée d'Italie, 69364 Lyon Cedex 07, France

E. Bocquillon
EP3 Physikaliches Institut, Universität Würzburg Am Hubland, 97074 Würzburg, Germany and Laboratoire Pierre Aigrain, Département de Physique de l'Ecole Normale Supérieure, 24 rue Lhomond, 75231 Paris Cedex 05, France

G. Fève
Laboratoire Pierre Aigrain, Département de Physique de l'Ecole Normale Supérieure, 24 rue Lhomond, 75231 Paris Cedex 05, France

Ch. Grenier
Centre de Physique Théorique (CPHT), Ecole Polytechnique, 91128 Palaiseau Cedex, France

P. Degiovanni
Université de Lyon, Fédération de Physique André Marie Ampère, CNRS, Laboratoire de Physique de l'Ecole Normale Supérieure de Lyon, 46 Allée d'Italie, 69364 Lyon Cedex 07, France

(Received 16 September 2013; published 11 November 2013)

Recent electron quantum optics experiments performed with on-demand single electron sources call for a mixed time/frequency approach to electronic quantum coherence. Here, we present a Wigner function representation of first-order electronic coherence and show that it provides a natural visualization of the excitations emitted by recently demonstrated single electron sources. It also gives a unified perspective on single particle and two particle interferometry experiments. In particular, we introduce a nonclassicality criterion for single electron coherence and discuss it in the context of Mach-Zehnder interferometry. Finally, the electronic Hanbury Brown and Twiss and the Hong-Ou-Mandel experiments are interpreted in terms of overlap of Wigner function, thus connecting them to signal processing.

DOI: 10.1103/PhysRevB.88.205303 PACS number(s): 73.23.−b, 71.10.Pm, 73.43.Lp

I. INTRODUCTION

Recent experiments have demonstrated the importance of single[1,2] and two particle[3–6] quantum coherence in the field of quantum-coherent electronics. The advent of on-demand single electron sources[7–13] has opened the way to a new generation of experiments dealing with excitations having a finite spatial extension and various shapes instead of a continuous stream of indistinguishable excitations. These experiments open the way to the controlled preparation, manipulation, and characterization of single to few electron excitations in ballistic conductors, an emerging field called electron quantum optics.[14] Since these experiments access time scales comparable to the coherence time of electrons within conductors through finite-frequency current[15,16] and noise measurements,[17,18] a time-resolved approach to electronic quantum coherence is required.

In this paper, we present a unified view of the various representations of single electron coherence in quantum Hall edge channels and we introduce in the present context a time/frequency representation based on the Wigner function already introduced in quantum mechanics[19] and signal processing.[20] The Wigner function is commonly used in quantum optics[21] and has been recently measured in cavity QED to demonstrate the decay of quantum superpositions of two quasiclassical states of the electromagnetic field.[22]

Although all the representations of electronic coherence contain exactly the same information, each of them has its advantages and drawbacks. First, the time domain representation of single electron coherence is suitable to analyze time-dependent aspects as well as to define the proper notions of coherence and dephasing times.[23] However, information on the electron or hole nature of excitations is hidden in the phase of this quantity. On the other hand, the frequency domain representation is perfect to discuss the nature of excitations and is the natural representation for the electronic analog of homodyne tomography[24] but it is not well suited to describe real time aspects. The mixed time/frequency representation called the electronic Wigner function combines the advantages of both representations: it gives a direct access to both the time evolution and energy content of single electron coherence. Moreover, it provides a natural nonclassicality criterion for single electron coherence and, for example, enables us to discuss nonclassicality in Mach-Zehnder interferometry in a natural way.

Historically, the Wigner function was introduced in the theory of quantum transport at the end of the 1980s to understand the limits of a semiclassical treatment in semiconductors,[25] to study phonon interaction effects,[26] and also to model various quantum devices built from semiconductors.[27,28] Although we deal with the same concept, we consider here low-dimensional conductors in which many-body effects as well as interactions and decoherence in the presence of the Fermi sea are crucial. Moreover, our primary motivation is to discuss the various representations of single electron coherence and show the

relevance of the electronic Wigner function for understanding electron quantum optics experiments.

The price to pay is that the electronic Wigner function, as of today, cannot be measured directly at a given time and frequency contrary to cavity QED experiment.[29,30] Nevertheless, we show that it provides a unified view of single electron interference experiments as well as of two-particle interference experiments based on the Hanbury Brown and Twiss[31] (HBT) effect. These include the Hong-Ou-Mandel (HOM) experiment[32] which involves two electron interferences from two different sources in full generality. Doing so, we greatly simplify the discussion of the various reconstruction protocols for single electron coherence. We show that the recently proposed tomography protocol[24] does indeed directly reconstruct the electronic Wigner function. Moreover, providing a natural visualization of single electron coherence, this approach suggests that specifically designed alternative tomography protocols may lead to single electron reconstruction from fewer measurements than our generic homodyne protocol. We finally sketch a possible connection between the search for such optimized tomography protocols and the problematic of compressed sensing in signal processing.[33]

This paper is structured as follows: In Sec. II, single electron coherence and its relation to Glauber coherence in quantum optics is revisited. We then discuss the time and frequency representations of this quantity and we introduce the electronic Wigner function. Section III is devoted to examples: We first consider single electron coherence in the presence of a classical voltage drive. The cases of a sinusoidal drive and of Lorentzian pulses[13,34] are discussed. We then discuss the electronic Wigner function emitted by the mesoscopic capacitor used as an on-demand single electron source.[8] Section IV is devoted to interferometry experiments, starting with Mach-Zehnder interferometry and then discussing the HBT and HOM two-particle interference experiments.

II. SINGLE ELECTRON COHERENCE

A. Definition and simple examples

Mach-Zehnder interferometry has shown the importance of first-order electron coherence. It is usually defined as the Keldysh Green function, already used to describe electronic coherence in the many-body approaches to the decoherence problem in diffusive conductors:[35]

$$\mathcal{G}^{(e)}_{\rho}(x,t;y,t') = \mathrm{Tr}[\psi(x,t)\rho\,\psi^{\dagger}(y,t')], \tag{1}$$

where ρ denotes the density operator of the electronic fluid. As noticed by Glauber *et al.*,[36] this correlator is also relevant for atom-counting experiments with fermionic cold atom systems. A similar quantity can be defined for hole excitations:

$$\mathcal{G}^{(h)}_{\rho}(x,t;y,t') = \mathrm{Tr}[\psi^{\dagger}(x,t)\rho\,\psi(y,t')]. \tag{2}$$

The electron and hole coherences at coincident times are related using the canonical anticommutation relations

$$\mathcal{G}^{(e)}(x,t;y,t) = \delta(x-y) - \mathcal{G}^{(h)}(y,t;x,t). \tag{3}$$

The first important difference with photon quantum optics comes from the fact that, in a metallic conductor, the Fermi sea, which plays here the role of the vacuum state, has a nonvanishing single particle coherence whereas coherence vanishes in the photon vacuum. At zero temperature, the Fermi sea single electron coherence within a single chiral channel at equal times is given by

$$\mathcal{G}^{(e)}_{\mu}(x,t;y,t) = \frac{i}{2\pi}\,\frac{e^{ik_F(\mu)(x-y)}}{y-x+i0^{+}}, \tag{4}$$

where $k_F(\mu)$ denotes the Fermi momentum associated with the chemical potential μ of the edge channel under consideration. At nonvanishing electronic temperature T_{el}, these correlators decay over the thermal length scale $l(T_{\mathrm{el}}) = \hbar v_F/k_B T_{\mathrm{el}}$ where v_F denotes the Fermi velocity:

$$\mathcal{G}^{(e)}_{\mu,T_{\mathrm{el}}}(x,t;y,t) = \frac{i}{2l(T_{\mathrm{el}})}\,\frac{e^{ik_F(\mu)(x-y)}}{\sinh\left(\frac{\pi(y-x)+i0^{+}}{l(T_{\mathrm{el}})}\right)}. \tag{5}$$

This suggests decomposing the single electron coherence into a Fermi sea contribution, due to the chemical potential μ of the conductor, and a contribution due to excitations above this ground state:[23,24]

$$\mathcal{G}^{(e)}_{\rho}(x,t;y,t') = \mathcal{G}^{(e)}_{\mu,T_{\mathrm{el}}}(x,t;y,t') + \Delta\mathcal{G}^{(e)}_{\rho}(x,t;y,t'). \tag{6}$$

The case of an ideal single electron excitation helps clarifying the physical meaning of $\Delta\mathcal{G}^{(e)}_{\rho}$. Let us consider a many-body state obtained from a Fermi sea by adding one extra particle in a normalized wave packet φ_e:

$$\psi^{\dagger}[\varphi_e]|F\rangle = \int_{-\infty}^{+\infty} \varphi_e(x)\,\psi^{\dagger}(x)\,|F\rangle\,dx, \tag{7}$$

where $|F\rangle$ denotes the Fermi sea at a fixed chemical potential. In momentum space, φ_e has only components on single particle states above the Fermi level. Then, Wick's theorem leads to single electron coherence at initial time:

$$\Delta\mathcal{G}^{(e)}_{\psi^{\dagger}[\varphi_e]|F\rangle}(x,0;y,0) = \varphi_e(x)\,\varphi_e^{*}(y). \tag{8}$$

In the same way, the single electron coherence of the state obtained by adding a single hole excitation to the Fermi sea $\psi[\varphi_h]|F\rangle$ [$\varphi_h(k) = 0$ above the Fermi level] is given by $\Delta\mathcal{G}^{(e)}_{\psi[\varphi_h]|F\rangle}(x,0;y,0) = -\varphi_h(x)\,\varphi_h^{*}(y)$. The minus sign reflects the fact that a hole is the absence of an electron in the Fermi sea.

The excess single electron coherence $\Delta\mathcal{G}^{(e)}_{\rho}(x,t;y,t)$ contains information on both the shape of the wave packet and its phase dependence. More precisely, $\Delta\mathcal{G}^{(e)}_{\rho}(x,t;x,t)$ encodes the average density and thus the shape of the wave packet whereas the $x-y$ dependence encodes the phase dependence. The shape of the wave packet gives access to its length (or duration in the time domain) which we denote by l_1 (resp. T_1).[23]

But a realistic single electron source does not necessarily emit a perfectly coherent wave packet: it can also emit a statistical mixture of them or the electrons may have experienced some decoherence due to Coulomb interactions.[37] How can we measure the decay of single electron coherence? As recently noticed by Haack *et al.*,[23] the first degree of coherence originally introduced by Mandel for photons[78] can be defined in the present context as

$$g^{(1)}(x,l) = \frac{\Delta\mathcal{G}^{(e)}_{\rho}\left(x+\frac{l}{2},x-\frac{l}{2}\right)}{\sqrt{\Delta\mathcal{G}^{(e)}_{\rho}\left(x+\frac{l}{2},x+\frac{l}{2}\right)\Delta\mathcal{G}^{(e)}_{\rho}\left(x-\frac{l}{2},x-\frac{l}{2}\right)}}. \tag{9}$$

To see how it gives a direct access to the decay of single electron coherence, let us consider a very simple description of decoherence which consists in introducing a phenomenological decoherence coefficient in front of the excess single electron coherence of a coherent wave packet:[37]

$$\Delta\mathcal{G}^{(e)}(x,y) \simeq \mathcal{D}(x-y)\,\varphi_e(x)\varphi_e(y)^*. \tag{10}$$

The decay length of this decoherence coefficient is denoted by l_ϕ and is called the dephasing length (the dephasing time in the time domain). Let us recall that such an approach to decoherence is justified only when the electron under consideration can still be distinguished from electron/hole pairs generated in the Fermi sea by Coulomb interactions. In this case, Eq. (10) can be obtained in a model of a single electron coupled to an harmonic environment.[38] Otherwise, a more complete approach should be used.[39] Nevertheless, using Eq. (10) into Eq. (9) shows that $g^{(1)}(x,l)$ decays over the same length scale l_ϕ as $\mathcal{D}(x-y)$.

It then follows from (9) that the length scale governing the decay of the single electron coherence $\Delta\mathcal{G}^{(e)}_\rho(x,y)$ combines the decaying length of the wave packet and l_ϕ:

$$\frac{1}{l_2} = \frac{1}{2l_1} + \frac{1}{l_\phi}. \tag{11}$$

This formula mimics the famous expression of the total decoherence rate in NMR in terms of the relaxation and dephasing rates.[23,40]

B. Analogy to Glauber's coherences

In Glauber's approach to photodetection,[41] a photon detector is a quantum device designed to detect a single photon. In such a detector, a single photon causes the photoionization of an atom and the emitted electron is then amplified to give a macroscopic signal. Old photomultipliers work exactly this way: the incoming photon is absorbed, leading to the emission of a single electron which is then amplified by the secondary emission of electrons in dynodes. The initial photoemission stage can be described using elementary time-dependent perturbation theory. The resulting photodetection signal is then obtained as

$$I_D(t) = \int_0^t K_D(\tau,\tau')\,\mathcal{G}^{(1)}_\rho(x_D,\tau;x_D,\tau')\,d\tau d\tau', \tag{12}$$

where x_D denotes the position of the detector. The quantity $\mathcal{G}^{(1)}_\rho(x_D,\tau|x_D,\tau')$ only depends on the quantum state of the electromagnetic field and is indeed Glauber's single photon coherence function;[42]

$$\mathcal{G}^{(1)}_\rho(x,\tau;x',\tau') = \mathrm{Tr}[E^{(+)}(x,\tau)\cdot\rho\cdot E^{(-)}(x,\tau')], \tag{13}$$

where $E^{(\pm)}$ denotes the positive (resp. negative) frequency part of the electric field operator and ρ is the electromagnetic field initial density operator. The function $K_D(\tau,\tau')$ characterizes the response of the detector to the absorption of a single photon. Broadband detectors have a local response in time $K_D(\tau-\tau') \simeq \delta(\tau-\tau')$ and therefore measure the (integrated) photocount: $I_D(t) \simeq \int_0^t \mathcal{G}^{(1)}_\rho(x_D,t';x_D,t')\,dt'$. On the other hand, narrow-band detectors select a single frequency and therefore measure the Fourier transform of Glauber's single photon coherence with respect to time.

The analogy between Glauber's single photon coherence in Eq. (13) and the single electron coherence function given by Eq. (1) is then obvious. But what would be the analog of photodetection for electrons? The idea is simply to extract an electron from the conductor we want to probe and to amplify the corresponding charge deposited into the detector. Naturally, the stage corresponding to photoionization is simply tunneling of electrons from the conductor into the detector which could for example be a STM tip or a nearby dot. Of course this approach does not take into account the electrostatic coupling between the conductor and the detector. Assuming a pointlike detector located at position x_D, the average tunneling current from the conductor to the detector contains two contributions arising from an electron transmitted from the conductor to the reservoir and vice versa:

$$I_D(t) = \int_0^t \big[\mathcal{G}^{(e)}_\rho(x_D,\tau;x_D,\tau')K_a(\tau,\tau') - \mathcal{G}^{(h)}_\rho(x_D,\tau;x_D,\tau')K_e(\tau,\tau')\big]d\tau d\tau'. \tag{14}$$

In this expression, K_a and K_e characterize the detector and respectively account for both available single electron and hole states within the reservoir and for the eventual energy filtering of the detector. Such a detection scheme has been recently implemented experimentally to study electron relaxation in quantum Hall edge channels:[43] in these experiments, a quantum dot is used to filter energies. This corresponds to a narrow-band detection in the quantum optics language.

C. Representations of single electron coherence

1. The time and frequency domains

Since measurements are usually performed locally, let us consider the single electron coherence function at a given position x: $\mathcal{G}^{(e)}_{\rho,x}(t,t') = \mathcal{G}^{(e)}_\rho(x,t;x,t')$. In the time domain, the diagonal $\mathcal{G}^{(e)}_{\rho,x}(t,t)$ is nothing but the average electronic density at time t and position x. Consequently, in chiral edge channels with Fermi velocity v_F, the excess current with respect to the chemical potential μ is

$$\langle i(x,t)\rangle_\rho = -ev_F\,\Delta\mathcal{G}^{(e)}_{\rho,x}(t,t). \tag{15}$$

The off-diagonal ($t \neq t'$) excess single electron coherence $\Delta\mathcal{G}^{(e)}_{\rho,x}(t,t')$ is complex valued.[23] Introducing $\bar{t} = (t+t')/2$ and $\tau = t-t'$, the decay of $|\Delta\mathcal{G}^{(e)}_{\rho,x}(t,t')|$ with increasing τ defines the coherence time of the source at time t. So this representation is indeed appropriate to discuss the coherence time as well as to discuss time dependence. But it is not well suited for understanding the nature (electron or hole) of the excitations emitted by the source since it is encoded in the $t-t'$ dependence of the phase of $\Delta\mathcal{G}^{(e)}_{\rho,x}(t,t')$.

Going to the frequency domain gives access to the nature of excitations. The single electron coherence in the frequency domain is defined as the double Fourier transform:

$$\widetilde{\mathcal{G}}^{(e)}_{\rho,x}(\omega_+,\omega_-) = \int \mathcal{G}^{(e)}_{\rho,x}(t,t')\,e^{i(\omega_+ t-\omega_- t')}\,dt\,dt'. \tag{16}$$

As shown in Fig. 1, the Fourier plane can then be divided into four quadrants. The (e) or electron quadrant defined by $\omega_+ > 0$ and $\omega_- > 0$ contains the contribution of excitations that correspond to single particle levels having positive energies

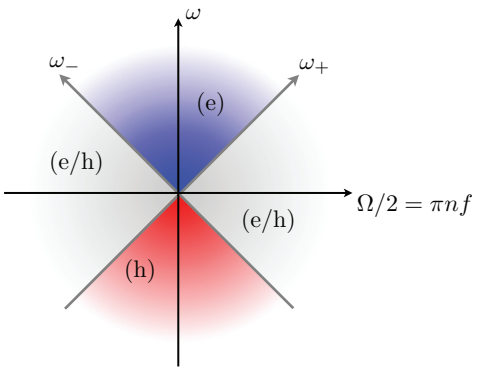

FIG. 1. (Color online) Decomposition of the Fourier plane (ω,Ω) in four quadrants. The (e) quadrant (in blue) represents the contribution of purely electronic excitations; the (h) quadrant (in red) represents the contribution of hole excitations. The two (e/h) quadrants (off-diagonal in gray) encode the contribution of electron/hole coherences. The diagonal ($\Omega = 0$, vertical axis) gives the electron occupation number. For a periodically driven source with period $T = 1/f$, Ω is a multiple of $2\pi n f$. Restricting the single electron coherence to the (e) [resp. (h)] quadrants and normalizing properly provides an effective density operator for electron (resp. hole) excitations.

with respect to the chemical potential $\mu = 0$. The (h) or hole quadrant defined by $\omega_+ < 0$ and $\omega_- < 0$ contains the contribution of excitations that correspond to single particle levels with negative energies with respect to the chemical potential $\mu = 0$. Finally, the (e/h) or electron/hole quadrants defined by $\omega_+\omega_- \leqslant 0$ correspond to the coherence between electronic and hole excitations. These coherences are produced by a superposition of electron and hole excitations.[24] At this point, it is worth emphasizing that the electronic or hole nature of excitations is defined with respect to a given chemical potential, here chosen as $\mu = 0$. With respect to another chemical potential, excitations would be categorized differently.

Using the Fourier decomposition of the single electron creation and destruction operators, the single electron coherence in the frequency domain satisfies

$$\frac{v_F}{2\pi}\,\widetilde{\mathcal{G}}^{(e)}_{\rho,x}(\omega_+,\omega_-) = \langle c^\dagger(\omega_-)\,c(\omega_+)\rangle_\rho\,, \tag{17}$$

where $c(\omega)$ and $c^\dagger(\omega)$ respectively denote the fermion destruction and creation operators at position x (see Appendix A). The electron occupation number can thus be recovered from the diagonal in the frequency domain. In particular, an equilibrium state corresponds to a singular single electron coherence in the frequency domain:

$$\widetilde{\mathcal{G}}^{(e)}_{\mu,T_{\rm el}}(\omega_+,\omega_-) = \frac{2\pi}{v_F}\delta(\omega_+ - \omega_-)\,f_{\mu,T_{\rm el}}\left(\frac{\omega_+ + \omega_-}{2}\right). \tag{18}$$

A convenient way to visualize the (ω_+,ω_-) plane[24] uses $\omega = (\omega_+ + \omega_-)/2$ and $\Omega = \omega_+ - \omega_-$ which are respectively conjugated to $t - t'$ and $(t + t')/2$. Figure 1 depicts the (e), (h), and (e/h) quadrants with respect to $\mu = 0$ in these coordinates.

The fact that, at zero temperature, the Fermi sea coherence (18) is localized in the frequency domain leads to Cauchy-Schwarz inequalities discussed in Appendix A. They imply that, at zero temperature, a source that does not emit any excess hole excitation (resp. electronic excitation) has nonvanishing single electron coherence only within the (e) [resp. (h)] quadrant.

To summarize, the frequency domain representation of the single electron coherence is clearly well suited to visualize the nature of excitations with respect to a given chemical potential. But recovering time dependence is more difficult since it is encoded in the phase dependance of the off-diagonal terms $\widetilde{\mathcal{G}}^{(e)}_{\rho,x}(\omega_+,\omega_-)$ for $\omega_+ \neq \omega_-$. Since it is difficult to detect a single electron in one shot on a subnanosecond time scale, it may be easier to access single electron coherence in the frequency domain than in the time domain[24] although a protocol has recently been proposed using Mach-Zehnder interferometry.[44] We shall come back to this question in Sec. IV.

However, working with sources that are able to inject single to a few electrons and holes strongly raises the need for a representation of the single electron coherence giving access to real time phenomenon as well as to the nature of excitations. Such a time/frequency representation has been known for a long time in quantum statistical physics: it is the Wigner function[19,20] which we now discuss for single electron coherence.

2. *The Wigner function*

In order to capture both the $\bar{t} = (t + t')/2$ dependence of single electron coherence and the nature of excitations, we define the Wigner distribution function as

$$W^{(e)}_{\rho,x}(\bar{t},\omega) = \int v_F\,\mathcal{G}^{(e)}_{\rho,x}(\bar{t} + \tau/2,\bar{t} - \tau/2)\,e^{i\omega\tau}\,d\tau, \tag{19}$$

which is dimensionless owing to the presence of the velocity v_F. In a similar way, one defines the Wigner function for the hole excitations by substituting $\mathcal{G}^{(h)}_{\rho,x}$ into (19). Note that due to the Hermiticity properties (A 1) of the single electron and single hole coherences, these Wigner functions are real.

Originally, the Wigner function was introduced to provide a bridge between classical and quantum mechanics for a single particle.[19] In classical mechanics, a particle has a well-defined position and momentum and an ensemble of such particles is represented by a probability distribution over phase space. In quantum mechanics, the uncertainty principle prevents the particle from being perfectly localized. Still, the Wigner distribution function is the proper generalization of the probability distribution: it is a real distribution over phase space whose integration over position (resp. momentum) gives the probability distribution of the momentum (resp. position). The Wigner function is thus normalized but contrarily to the classical probability distribution, it is not always positive.

Significant differences are expected for the Wigner function associated with single electron coherence. In the stationary case, the Wigner function defined by Eq. (19) is nothing but the time-independent electronic distribution function at position x:

$$W^{(e)}_{\rho,x}(\bar{t},\omega) = f_e(\omega,x). \tag{20}$$

For a Wigner function to be interpreted as a time-dependent electronic distribution function, it has to satisfy $0 \leqslant W^{(e)}_{\rho,x}(\bar{t},\omega) \leqslant 1$. The positivity condition is needed in order to have an interpretation as a probability density. In a chiral

system, the electronic and hole Wigner distributions are related by

$$W^{(h)}_{\rho,x}(\bar{t},\omega) = 1 - W^{(e)}_{\rho,x}(\bar{t},-\omega), \tag{21}$$

where the minus sign in front of ω on the right-hand side reflects the fact that $W^{(h)}_{\rho,x}(\bar{t},\omega)$ is the Wigner function for hole excitations at time $\bar{t}$ and energy $\hbar\omega$. Consequently, the upper bound on $W^{(e)}_{\rho,x}(\bar{t},\omega)$ is also required for a probabilistic interpretation of the hole Wigner distribution function. For a probability distribution in the $(\bar{t},\omega)$ plane, this upper bound expresses the Pauli principle.

In full generality, the Wigner function for conduction electrons in a metal contains the Fermi sea: $W^{(e)}_{\rho,x}(\bar{t},\omega) \to 1$ for sufficiently negative ω and $W^{(e)}_{\rho,x}(\bar{t},\omega) \to 0$ at high enough energy. In between, the Wigner function can get various values, sometimes negative or larger than 1. In such cases, it cannot be interpreted as a probability distribution. We shall come back to this issue while discussing explicit examples in the next section.

Note that a T-periodic system generates a single electron distribution invariant in $(t,t') \mapsto (t+T,t'+T)$ which can thus be decomposed as a Fourier transform with respect to $\tau = t - t'$ and a Fourier series with respect to $\bar{t} = (t+t')/2$:

$$\mathcal{G}^{(e)}_{\rho}(t,t') = \sum_{n=-\infty}^{+\infty} e^{-2\pi i n f \bar{t}} \int \mathcal{G}^{(e)}_{\rho,n}(\omega) e^{-i\omega\tau} \frac{d\omega}{2\pi}, \tag{22}$$

where $f = 1/T$ is the driving frequency. This single electron coherence leads to a T-periodic Wigner function, $W^{(e)}_{\rho}(\bar{t}+T,\omega) = W^{(e)}_{\rho}(\bar{t},\omega)$, whose expression as a Fourier series reads

$$W^{(e)}_{\rho}(\bar{t},\omega) = \sum_{n=-\infty}^{+\infty} v_F \mathcal{G}^{(e)}_{\rho,n}(\omega)\, e^{-2\pi i n f \bar{t}}, \tag{23}$$

in which the position x has been dropped out for simplicity. As we shall see, this expression is of great use in numerical evaluations of the Wigner function in the framework of Floquet scattering theory.

Integrating the Wigner function of a quantum particle over position or momentum gives the probability distribution of the conjugated variable. Here, partial integrals of the Wigner function give access to physically relevant quantities such as the average excess current with respect to a chemical potential μ:

$$\langle i(x,\bar{t})\rangle_{\rho} = -e \int \Delta W^{(e)}_{\rho,x}(\bar{t},\omega) \frac{d\omega}{2\pi}, \tag{24}$$

where $\Delta W^{(e)}_{\rho,x}(\bar{t},\omega)$ denotes the excess Wigner function with respect to the Wigner function $\Theta(\mu/\hbar - \omega)$ of the Fermi sea at chemical potential μ. Note that measuring this quantity requires broadband high-frequency measurements.[15,16] In the same way, averaging over time gives access to the electronic distribution function at position x:

$$f_e(\omega,x) = \frac{1}{T}\int_{-T/2}^{T/2} W^{(e)}_{\rho,x}(\bar{t},\omega)\, d\bar{t}. \tag{25}$$

This quantity can be measured using dc current measurements through an adjustable energy filter.[43] Note that the Wigner function for electrons in a conductor does not satisfy the normalization condition satisfied by the Wigner function of a single quantum particle: integrating over $\bar{t}$ and ω the excess Wigner distribution $\Delta W^{(e)}_{\rho,x}(\bar{t},\omega)$ with respect to a given chemical potential gives the total excess charge in $-e$ units.

Finally, let us point out that as of today, there is no way to directly access the value of the Wigner function at a given point (t,ω) in a quantum conductor. By contrast, such direct measurements of the Wigner function in cavity QED are possible and have indeed been performed[45] but they rely on the measurement of the parity of the photon number,[29] the equivalent of which is, as far as we know, not accessible in electron quantum optics. The problem of reconstructing the Wigner function for electrons in quantum Hall edge channels through interferometry experiments will be discussed in Sec. IV.

III. EXAMPLES

Let us now discuss several important examples of single electron coherences emitted by various electronic sources. We shall first consider the single electron coherence emitted by a driven Ohmic contact.

A. Voltage drives

1. General properties

The single electron coherence emitted by an ideal Ohmic contact driven by a time-dependent voltage $V(t)$ is

$$\mathcal{G}^{(e)}_{V}\left(t+\frac{\tau}{2},t-\frac{\tau}{2}\right) = \exp\left(\frac{ie}{\hbar}\int_{t-\frac{\tau}{2}}^{t+\frac{\tau}{2}} V(\tau')\,d\tau'\right)\mathcal{G}^{(e)}_{\mu}(\tau). \tag{26}$$

In the case of a T-periodic potential, the single electron coherence can be obtained in terms of the photon-assisted transition amplitudes $p_l[V_{\rm ac}]$ associated with the ac component of the drive.[13] The resulting Wigner function is then expressed as

$$W^{(e)}(t,\omega) = \sum_{(n_+,n_-)\in\mathbb{Z}^2} p_{n_+}[V_{\rm ac}]\, p_{n_-}[V_{\rm ac}]^*\, e^{2\pi i(n_- - n_+)ft} \times f_{\bar{\mu}}(\omega - \pi(n_+ + n_-)f), \tag{27}$$

where $\bar{\mu} = \mu - eV_{\rm dc}$ denotes the chemical potential shifted by the dc component of the drive. The electronic occupation number is obtained by averaging Eq. (27) over the time t. This selects terms with $n_+ = n_-$, thus leading to

$$f_e(\omega) = \sum_{n\in\mathbb{Z}} |p_n[V_{\rm ac}]|^2 f_{\bar{\mu}}(\omega - 2\pi n f). \tag{28}$$

This expression clearly shows the interpretation of the $|p_n[V_{\rm ac}]|^2$ as the probabilities of photon-assisted transitions. However, the Wigner function contains more information than the photon-assisted probabilities. These are the terms with $n_+ \neq n_-$ in Eq. (27) which are sensitive to the phases of the photon-assisted transition amplitudes. They play a crucial role in ensuring that the current noise of the driven channel is equal to the current noise at thermal equilibrium as expected for a coherent state of the edge magnetoplasmon modes.[46]

In the case of a sinusoidal drive $V_{\rm ac}(t) = V_0 \cos(2\pi f t)$ at frequency f, $p_n[V_{\rm ac}] = J_n(eV_0/hf)$, where J_n denotes the Bessel function of order n. The Wigner function is then

obtained as

$$W^{(e)}(t,\omega) = \sum_{n\in\mathbb{Z}} \frac{J_n\left(\frac{2eV_0}{hf}\cos(2\pi f t)\right)}{e^{\beta_{\rm el}\hbar(\omega+\pi n f)}+1}, \tag{29}$$

where $\beta_{\rm el} = 1/k_B T_{\rm el}$. At zero temperature, this Wigner function exhibits singularities in the variable ω each time $\hbar\omega$ is a multiple of $hf/2$. Quantum effects are expected to be dominant in the regime of low temperature and low photon number. On the contrary, for large photon number and high temperature, quantum features are expected to be small. Let us now turn to these two limiting regimes of small ($eV_0 \ll hf$) and large ($eV_0 \gg hf$) amplitude.

2. Small amplitude

The regime of small amplitude is most suitably discussed in the sinusoidal case. Then, hf represents the energy of photons absorbed or emitted by the electron gas and the condition $eV_0 \ll hf$ expresses that the physics is dominated by single photon processes. In this regime, the first-order contribution in eV_0/hf to the Wigner function is

$$\left.\frac{\partial W^{(e)}(t,\omega)}{\partial(eV_0/hf)}\right|_{V_0=0} = F_{\mu,T_{\rm el}}(\omega)\cos(2\pi f t), \tag{30}$$

where $F_{\mu,T_{\rm el}}(\omega) = f_{\mu,T_{\rm el}}(\omega-\pi f) - f_{\mu,T_{\rm el}}(\omega+\pi f)$ is, at zero temperature, the characteristic function of the interval $[\mu/\hbar - \pi f, \mu/\hbar + \pi f]$. Note that this contribution does not affect the electronic occupation number $f_e(\omega)$ but contributes to the average current by $(e^2/h)V(t)$ as expected from the linear response of a chiral edge channel. However, as we shall see in Sec. IV B, it is a basic ingredient of proposed single electron tomography protocol.[24]

The first nontrivial contribution to the electron distribution function arises at second order in V_0 and corresponds to processes in which a single photon is absorbed to promote one electron from the Fermi sea above the Fermi level:

$$\left.\frac{\partial^2 W^{(e)}(t,\omega)}{\partial^2(eV_0/hf)}\right|_{V_0=0} = g_{\bar\mu,T_{\rm el}}(\omega)\,\cos^2(2\pi f t), \tag{31}$$

where $g_{\bar\mu,T_{\rm el}}(\omega) = f_{\bar\mu,T_{\rm el}}(\omega+2\pi f) + f_{\bar\mu,T_{\rm el}}(\omega-2\pi f) - 2f_{\bar\mu,T_{\rm el}}(\omega)$ is, at zero temperature, equal to 1 for $\bar\mu < \hbar\omega \leqslant \bar\mu + hf$, equal to -1 when $\bar\mu - hf \leqslant \hbar\omega < \bar\mu$ and vanishes everywhere else.

At higher amplitude, multiphotonic processes contribute. At zero temperature, the Wigner function exhibits singularities for ω multiple of πf but only the even multiples contribute to singularities in the occupation number as expected from the theory of photon-assisted noise.[47]

3. Large amplitude

Let us now turn to the opposite regime of large voltage amplitude where the physics is dominated by multiphotonic processes. In this case, let us make the discussion slightly more general by considering a smooth time-dependent periodic voltage drive that varies on a scale $\Delta V = \max[V(t)] - \min[V(t)]$ over a time scale $T = 1/f$, where f denotes the driving frequency.

To discuss the features of the Wigner function on energy scales of the order $e\Delta V$, we have to consider $\mathcal{G}^{(e)}(t+\tau/2, t-\tau/2)$ over time scales such that $|f\tau| \ll 1$. We can then assume that $V(\tau')$ is constant and equal to $V(t)$ between $t-\tau/2$ and $t+\tau/2$. This immediately leads to an adiabatic expression for the Wigner function as a time-dependent Fermi distribution:

$$W^{(e)}(t,\omega) \simeq f_{\mu,T_{\rm el}}(\omega + eV(t)/\hbar) \tag{32}$$

corresponding to a time-dependent chemical potential $\mu(t) = \mu - eV(t)$. However, at zero temperature, quantum interference effects lead to quantum corrections to this expression. They arise from the time dependence of the voltage drive over the interval $[t-\tau/2, t+\tau/2]$. Considering a time t such that $V''(t) \neq 0$, the ω dependence of $W^{(e)}(t,\omega)$ exhibits a Fresnel-like diffraction pattern. At zero temperature, assuming that $V''(t) > 0$, we find

$$W^{(e)}(t,\omega) \simeq \int_{\frac{\omega+eV(t)}{\delta\omega(t)}}^{+\infty} {\rm Ai}(x)\,dx, \tag{33}$$

where ${\rm Ai}(x)$ denotes the Airy function[48] and

$$\delta\omega(t) = \frac{1}{2}\left(\frac{e|V''(t)|}{\hbar}\right)^{1/3}. \tag{34}$$

The Wigner function thus exhibits quantum ripples on the Fermi plateau around the value 1 and an exponential decay at high energy. These ripples are clearly visible in Fig. 2(a) showing the Wigner function generated by a sinusoidal drive for $eV_0/hf = 20$ at zero temperature. On this figure, they appear as oscillations on the top part of the waves of the driven Fermi sea [the semiclassical potential is $\mu(t) = \mu - eV(t)$ and therefore $V''(t) > 0$ corresponds to $\mu''(t) < 0$]. Due to them, the Wigner function can be greater than 1. For $V''(t) < 0$, a similar computation shows that

$$W^{(e)}(t,\omega) \simeq \int_{-\infty}^{-\frac{\omega+eV(t)}{\delta\omega(t)}} {\rm Ai}(x)\,dx. \tag{35}$$

On Fig. 2(a), the corresponding ripples correspond to the oscillations in the bottom of the wave part of the driven Fermi sea. They lead to negative values of the Wigner function.

The energy scale $\hbar\,\delta\omega(t)$ associated with these ripples compares to hf through

$$\frac{\hbar\,\delta\omega(t)}{hf} = \frac{1}{4\pi}\left(\frac{2\pi e T^2|V''(t)|}{hf}\right)^{1/3}. \tag{36}$$

For a moderately varying voltage such as a sinusoidal drive, $T^2V''(t)$ is of the order of the total drive amplitude ΔV. Therefore in the case of a large amplitude $e\Delta V \gg hf$, the scale $\hbar\,\delta\omega(t)$ is significantly larger than hf as can already be seen in Fig. 2(a).

When $\hbar\,\delta\omega(t) \gg hf$, this energy scale gives the temperature above which the quantum ripples disappear. A convenient way to understand finite-temperature effects is to remark that thermal fluctuations will smooth the Wigner function over an energy scale equal to $k_B T_{\rm el}$. The quantum ripples are thus expected to disappear at finite temperature, when $k_B T_{\rm el} \gtrsim \hbar\,\delta\omega(t)$. In this regime, the adiabatic result given by Eq. (32) is recovered as can be seen from Fig. 2(b).

Finally, one might consider a voltage drive that is strongly peaked around specific times. In this case, the local energy scale $\hbar\,\delta\omega(t)$ might become of the order of $eV(t)$ itself and

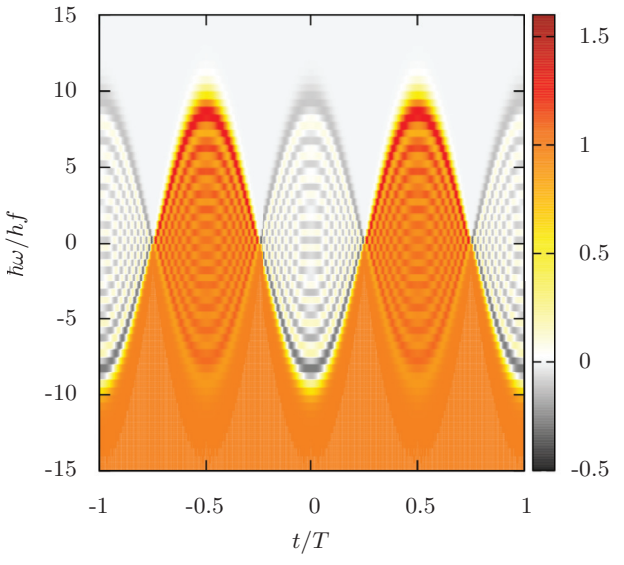

(a) $T_{\rm el} = 0$ K

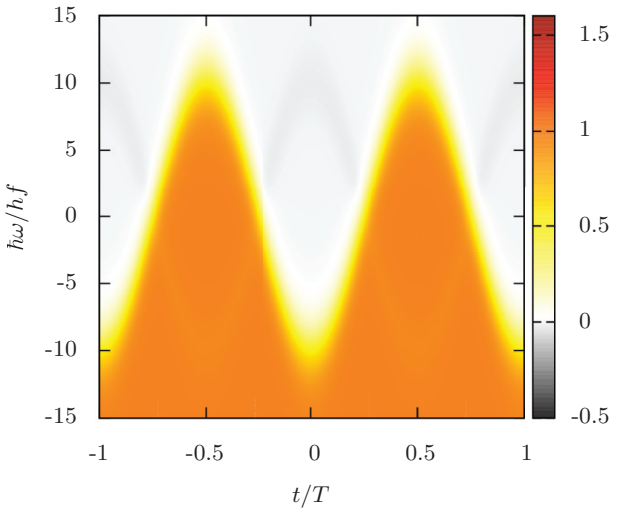

(b) $T_{\rm el} = 0.25eV_0/k_B$

FIG. 2. (Color online) Density plot of the Wigner function for a sinusoidal drive $V(t) = V_0 \cos(2\pi ft)$ in terms of t/T and $\hbar\omega/hf$ for $eV_0/hf = 10$ at (a) zero temperature and (b) $k_B T_{\rm el} = eV_0/4$. Quantum ripples discussed in the text are visible at $T_{\rm el} = 0$ K. The pixelization corresponding to the scale $\hbar\omega/hf = 0.5$ is also only visible on graph (a) at zero temperature.

the Wigner function is locally dominated by these interference effects. In such a situation, one would not be able to see the overall picture of the Fermi step at chemical potential $\bar{\mu}(t) = \mu - eV(t)$. As we shall see in Sec. III B2, Lorentzian pulses realize such a situation.

B. Single electron sources

1. The mesoscopic capacitor

An on-demand single electron source can be realized using a mesoscopic capacitor operated in the nonlinear regime. This source was demonstrated in 2007 by Fève *et al.*[8] Properly operated, it emits a single electron and a single hole excitation per period at GHz repetition rate. One of its main advantages is that these excitations are energy resolved and that their average energies and width can be tuned to some extent.

A description of this source can be achieved within a non-interacting electron approximation using the framework of the Floquet scattering theory. This approach has been developed by Moskalets and Büttiker to describe quantum mechanical pumping in mesoscopic conductors[49] and since then has been applied to a variety of systems among which is the mesoscopic capacitor.[50] In particular it has been used to predict the low- and finite-frequency noise emitted by a periodically driven mesoscopic conductor.[51,52] These theoretical results have been compared to experimental results on finite-frequency noise of the source.[53] The Floquet scattering amplitude for electrons propagating through a driven quantum conductor is

$$\mathcal{S}_{\rm Fl}(t,t') = \exp\left(\frac{ie}{\hbar}\int_{t'}^{t} V_d(\tau)\,d\tau\right)\mathcal{S}_0(t-t'), \tag{37}$$

where $V_d(\tau)$ is the periodic ac driving voltage applied to the dot and $\mathcal{S}_0(t-t')$ is the scattering amplitude across the undriven conductor, expressed in real time. Knowing the Floquet scattering amplitude (37) leads to the real time single electron coherence emitted by the driven mesoscopic conductor[24] in terms of the Floquet scattering amplitudes $\mathcal{S}_n(\omega)$ defined as

$$c_{\rm out}(\omega) = \sum_{n=-\infty}^{+\infty} \mathcal{S}_n(\omega)\, c_{\rm in}(\omega + 2\pi nf). \tag{38}$$

A Fourier transform then leads to the general expression for the Wigner function emitted by a source described within the framework of Floquet scattering theory:

$$W^{(e)}(t,\omega) = \sum_{n,k=-\infty}^{+\infty} \mathcal{S}_k(\omega + \pi nf)\mathcal{S}_{n+k}(\omega - \pi nf)^* \times f_\mu(\omega + 2\pi f(k + n/2))\, e^{-2\pi inft}. \tag{39}$$

This expression can be used to compute either analytically or numerically the Wigner function within Floquet scattering theory.

Let us now discuss the numerical results for the mesoscopic capacitor driven by a square voltage: $V(t) = V_d$ for $0 < t \leqslant T/2$ and $V(t) = -V_d$ for $T/2 < t \leqslant T$. We namely consider realistic values of the parameters of the mesoscopic capacitor: $hf/\Delta = 0.06$, $k_B T_{\rm el}/\Delta = 0.01$, and $eV_d = \Delta/2$ so that the voltage step corresponds to the level spacing of the dot Δ. These results are obtained by evaluating the single electron coherence numerically using a specific form for the scattering amplitude of the dot $\mathcal{S}_0(\omega)$ already used to interpret the experimental data:[15]

$$\mathcal{S}_0(\omega) = \frac{\sqrt{1-D} - e^{2\pi i\hbar(\omega-\omega_0)/\Delta}}{1 - \sqrt{1-D}\, e^{2\pi i\hbar(\omega-\omega_0)/\Delta}}. \tag{40}$$

Here D denotes the dot to lead transmission controlling the tunneling between the dot and the chiral edge channel. Another tunable parameter is the position $\hbar\omega_0$ of the energy levels of the dot which can be controlled by applying a dc voltage to its top gate. Note that electron/hole symmetry is realized when $\hbar\omega_0$ is an integer multiple of Δ. Depending on D, various behaviors are expected.

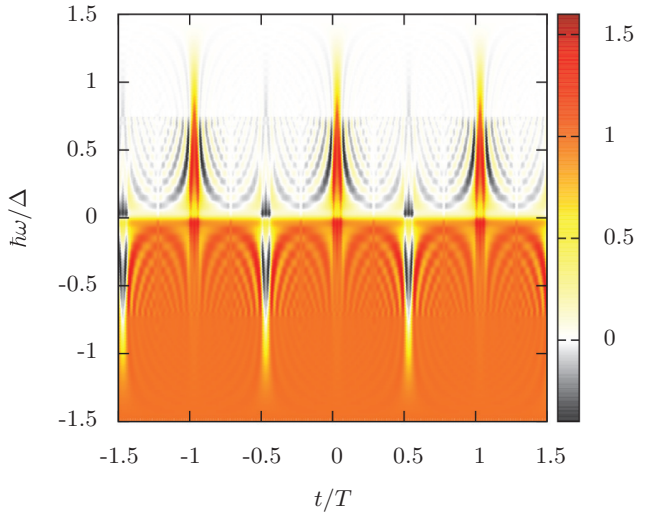

FIG. 3. (Color online) Density plot of the Wigner function emitted by the mesoscopic capacitor at $D = 1$, $hf/\Delta = 0.06$, $k_B T_{\rm el}/\Delta = 0.01$ and for a square voltage drive of amplitude $eV_d = \Delta/2$ in the symmetric situation ($\omega_0 = 0$).

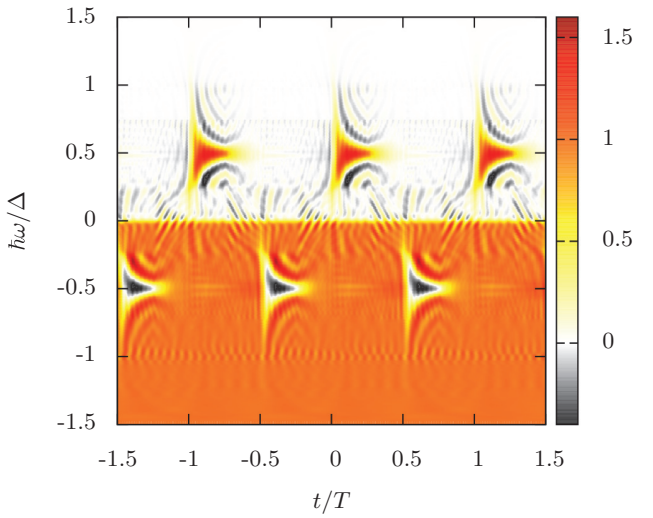

FIG. 4. (Color online) Density plot of the Wigner function emitted by the mesoscopic capacitor at $D = 0.4$, $hf/\Delta = 0.06$, $k_B T_{\rm el}/\Delta = 0.01$ and for a square voltage drive of amplitude $eV_d = \Delta/2$ in the symmetric situation ($\omega_0 = 0$).

At $D = 1$, electrons go around the dot only once and feel the effect of the voltage drive during a very short time τ_0 which is the time of flight around the dot. As shown on Fig. 3, excitation emission is concentrated at the times where the voltage drive changes. This is expected since it is precisely when the drive changes that the electrons going through the dot feel a sudden change of the electrical potential. Between two changes, the dot acts as a purely elastic scatterer and therefore we expect to see the emission of electrons as if they were coming straight out of the reservoir. Consequently, the average current should be a succession of current pulses of duration τ_0 centered on the sudden changes of the voltage drive.

From an edge magnetoplasmon perspective, the state generated by the mesoscopic capacitor at $D = 1$ is a coherent state. It is a coherent superposition of many electron/hole pairs and therefore the single electron coherence is expected to have an important contribution in the (e/h) quadrants. We thus expect that excitations are created close to the Fermi level as can be seen on Fig. 3.

When D decreases, the density of states within the dot becomes more and more textured.[8] Consequently we expect the source to emit electron and hole excitations that are better and better resolved in energy and time shifted by a half period. Figure 4 confirms this physical picture: it clearly shows the succession of electronic and hole excitations emitted by the mesoscopic capacitor near its optimal point.

The shape of these pulses can indeed be understood very simply by considering Lorentzian wave packets in energy, truncated to energies above the Fermi level:

$$\widetilde{\varphi}_e(\omega) = \frac{\mathcal{N}_{\rm e}\,\Theta(\omega)}{\omega - \omega_{\rm e} - i\gamma_{\rm e}/2}, \tag{41}$$

where $\mathcal{N}_{\rm e}$ ensures normalization and $\gamma_{\rm e}$ denotes the electron escape rate from the quantum dot. For $|\hbar\omega_0| < \Delta$, we expect the electron to be emitted by the mesoscopic capacitor at energy $\hbar\omega_{\rm e} = \Delta/2 + \hbar\omega_0$ whereas the hole is expected at energy $\hbar\omega_{\rm h} = \hbar\omega_0 - \Delta/2$. The electronic escape rate is then given by[54,55] $\gamma_{\rm e} = 2D\Delta/h(2-D)$.

To understand the limit $\gamma_{\rm e}/\omega_{\rm e} \ll 1$, let us first neglect the truncation of the wave packet. Within this approximation, the associated excess Wigner function is given by

$$\Delta W^{(e)}(t,\omega) \sim 2\gamma_{\rm e}\Theta(t)\frac{\sin\left[2(\omega-\omega_{\rm e})t\right]}{\omega-\omega_{\rm e}}\,e^{-\gamma_{\rm e}t}. \tag{42}$$

This expression leads to a triangular shape which reflects the Heisenberg time/energy uncertainty principle: right after emission, the spreading in energy is large and then becomes sharper. As expected the duration of the excitation is governed by $\tau_{\rm e} = 1/\gamma_{\rm e}$. This Wigner function also exhibits some negative values appearing as dark quantum ripples on Fig. 5(b) but apart from these, it is mainly a positive bump. Taking into account the truncation of the Lorentzian in Eq. (41) alters this image at low energy: it leads to the vanishing of the single electron coherence outside the (e) quadrant as shown on Fig. 5(a). Consequently, for $\omega \lesssim \omega_{\rm e}/2$, the Fourier transform of $\Delta W^{(e)}(t,\omega)$ with respect to t is much smaller for pulsation lower than $\omega_e/2$ as can be seen on Fig. 5(b). The residual interference pattern shows broader and fainter fringes as ω goes to zero. These time oscillations at fixed ω arise from the residual coherence in the (e) quadrant ($\omega_\pm > 0$) and $\omega_+ + \omega_- = 2\omega$.

This explains the band seen for $|\omega| \lesssim \Delta/2$ on Fig. 4 for $|\omega| \lesssim |\omega_{\rm e}|/2$: the positive bump gives way to a fainter pattern of interferences fringes. This truncation effect, which can be interpreted as an expression of the Pauli principle, is of course sharper when $\gamma_{\rm e} \ll \omega_{\rm e}$. Its consequences in the time domain are discussed in Appendix B. The same remarks apply to hole excitations which appear as dips in the Fermi sea.

When decreasing D, the escape times of the electron and hole increase as one enters the shot noise regime of the source. When they become comparable to the half period $T/2$, the electron and the hole do not have the time to escape before the voltage drive changes again. In this case,

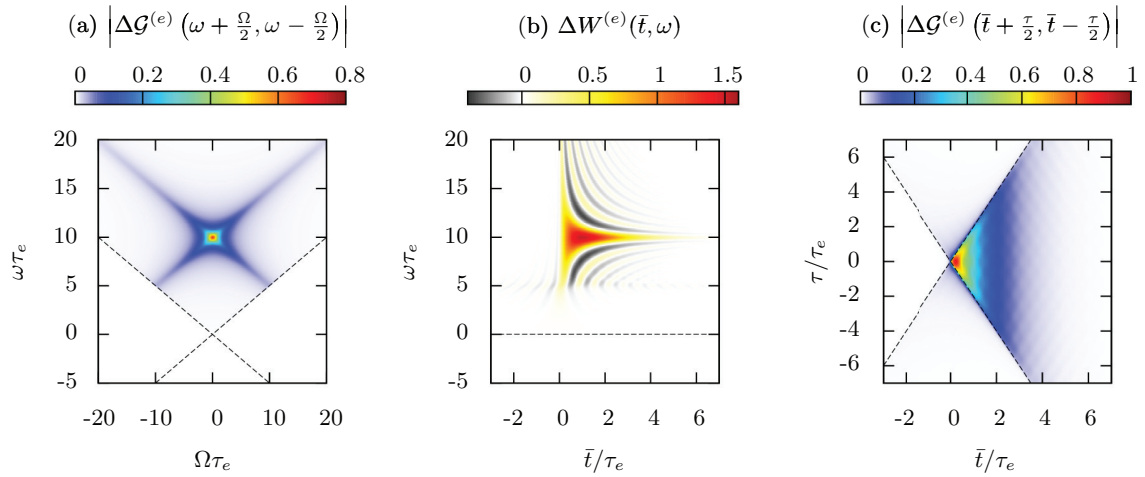

FIG. 5. (Color online) Density plots associated with the three representations of single electron coherence: (a) $|\Delta\mathcal{G}^{(e)}(\omega+\frac{\Omega}{2},\omega-\frac{\Omega}{2})|$, the frequency domain representation [dashed lines delimit the (e), (h), and (e/h) quadrants]. (b) $\Delta W^{(e)}(\bar{t},\omega)$, the Wigner function representation (horizontal dashed line is the Fermi level). (c) $|\Delta\mathcal{G}^{(e)}(\bar{t}+\frac{\tau}{2},\bar{t}-\frac{\tau}{2})|$, the time domain representation (dashed lines correspond to $t=0$ and $t'=0$). These density plots correspond to an energy-resolved electronic wave packet given by (41) with $\omega_e\tau_e=10$.

electron/hole coherences are expected to reappear since the capacitor generates a superposition of various electron/hole pair excitations of the form[24] $|F\rangle+\psi^\dagger[\varphi_e]\psi[\varphi_h]|F\rangle$. The (e/h) coherences for such a superposition are of the form $\varphi_e(t)\varphi_h^*(t')$ and $\varphi_h(t)\varphi_e^*(t')$. In the Wigner distribution function, they appear at $\omega\simeq(\omega_e+\omega_h)/2$ and oscillate in time at pulsation $\omega_e-\omega_h$ (remember that $\omega_e>0$ for an electronic excitation and $\omega_h<0$ for a hole excitation). We thus expect fast oscillations in time at mid position between the electron and hole energies.

To confirm this picture, Fig. 6 depicts the Wigner function emitted by the mesoscopic capacitor in the low-D regime with a shift in the energy levels of the dot ($\omega_0\neq 0$). As expected, it exhibits fast oscillations precisely at the mid position between the electron and hole peaks. Note also how the triangular shape

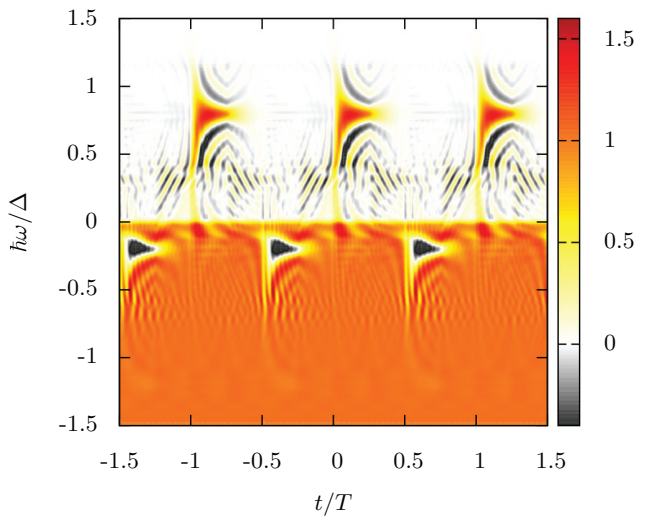

FIG. 6. (Color online) Density plot of the Wigner function emitted by the mesoscopic capacitor as a function of t/T and $\hbar\omega/\Delta$ for $D=0.4$, $k_BT_{el}/\Delta=0.01$, $hf/\Delta=0.06$ and when the energy levels of the dot are shifted by 0.3Δ.

of the hole excitation dips are truncated close to the Fermi surface due to the Pauli exclusion principle. Note that such oscillations are also visible in Fig. 4 but they are exactly at the Fermi energy since for this figure, the capacitor is assumed to be operated at an electron/hole symmetric point.

2. *Lorentzian pulses*

More recently, another source of single to a few electronic excitations in a 2DEG at zero magnetic field has been developed[34] based on ideas by Levitov, Ivanov, Lee, and Lesovik.[56,57] The idea is to use Lorentzian voltage pulses carrying a quantized charge in units of e to generate purely electronic excitations. Experimentally, minimizing the partition noise of these excitations is used to minimize the production of spurious electron/hole pairs.[13,58] Contrary to the excitations studied in the previous paragraph, these electron pulses are not well separated from the Fermi sea: their spectral weight is concentrated near the Fermi energy. Moreover, excitations carrying more than an elementary charge under the form of a coherent wave packet of n electrons can be generated. More precisely, such an excitation is a Slater determinant built from the $1\leqslant k\leqslant n$ mutually orthogonal electronic wave functions given by[46]

$$\varphi_k^{(\tau_0)}(\omega)=\sqrt{2\tau_0}\,\Theta(\omega)e^{-\omega\tau_0}L_{k-1}(2\omega\tau_0), \tag{43}$$

where τ_0 denotes the duration of the Lorentzian pulse and L_k is the kth Laguerre polynomial.[48] Their single electron coherence can be computed analytically in the case of a single pulse and also from the Floquet scattering theory in the case of a periodic train of pulses.[46]

For a single Levitov excitation of charge $-ne$ ($n\geqslant 1$) and width τ_0, the associated excess Wigner function is given by

$$\Delta W^{(e)}(t,\omega)=\sqrt{4\pi}\Theta(\omega)e^{-2\omega\tau_0}\sum_{k=0}^{n-1}\sum_{l=0}^{k}\left(\frac{2\omega\tau_0}{\sqrt{\omega t}}\right)^{2l+1}\times\frac{L_{k-l}^{(2l)}(4\omega\tau_0)}{l!}J_{l+\frac{1}{2}}(2\omega t), \tag{44}$$

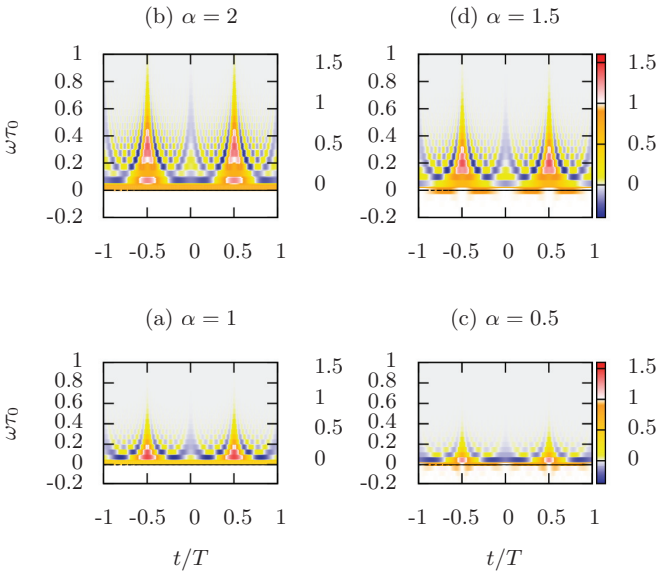

FIG. 7. (Color online) Density plot of the Wigner functions of trains of Lorentzian pulses of width τ_0 such that $f\tau_0 = 0.05$, at zero electronic temperature and for increasing values of α: (a) $\alpha = 1$, (b) $\alpha = 2$, (c) $\alpha = 0.5$, (d) $\alpha = 1.5$. The thin horizontal black line corresponds to the Fermi level. The same color map applies to all the graphs: negative values are depicted in blue tones, values over 1 in red tones. The unit value is in white to emphasize the hole contributions for noninteger values of α [see (c) and (d)].

where $J_{l+\frac{1}{2}}$ denotes the Bessel function of order $l + 1/2$ and $L_n^{(m)}$ is the generalized Laguerre polynomial[48] of order n. Note that for $n = 1$, the wave function $\varphi_0^{(\tau_0)}$ being exponential in energy, one expects the Wigner distribution function to have a form similar to that of Eq. (42) up to the exchange of t and ω.

However, in order to discuss the physics of these Lorentzian pulses, it is more convenient to consider a periodic train of excitations since, in this case, noninteger values of the charge can easily be considered.[13,46] Using Eq. (39), we plot the Wigner function of a train of Lorentzian pulses $f\tau_0 = 0.05$ at zero temperature and for increasing values of α which denotes the average charge per pulse in units of $-e$.

Figure 7 shows trains of time-resolved excitations that are not separated in energy from the Fermi level (compare with Fig. 4) as expected. Time-energy uncertainty leads to the spreading of the excitation in time close to the Fermi surface. Increasing the amplitude of the drive or equivalently α, we see that these excitations grow in the energy direction. We also see the appearance of local maxima that are indeed the quantum ripples discussed in Sec. III A3. But in the present case, they are more prominent since we are not in an adiabatic limit in the sense of Sec. III A3. More interesting, we see that the Fermi sea is left pristine each time α is an integer confirming that for positive integer α, the source is emitting a train of purely electronic excitations.

On the contrary, when $\alpha > 0$ is not an integer, hole excitations are expected since in this case, each pulse should be understood as a collective excitation. Comparing $\alpha = 1/2$ and $\alpha = 3/2$, we see that the hole contribution diminishes: this is not surprising in view of the Pauli principle since one adds a half electronic excitation on top of a Slater determinant in which more and more electronic states close to the Fermi level are populated.

IV. INTERFEROMETRY

Let us now discuss interferometry experiments, starting first with single particle interferences (Mach-Zehnder interferometry) and then going to two-particle interferometry experiments based on the Hanbury Brown and Twiss effect.

A. Mach-Zehnder interferometry

We consider a Mach-Zehnder interferometer built from two QPCs A and B (see Fig. 8) whose scattering matrices $S^{(j)}$ ($j = A, B$) are of the form

$$S^{(j)} = \begin{pmatrix} \sqrt{1-T_j} & i\sqrt{T_j} \\ i\sqrt{T_j} & \sqrt{1-T_j} \end{pmatrix}. \tag{45}$$

The two arms of the MZI encircle a region threaded by a magnetic flux $\Phi_B = \phi_B \times (h/e)$. The length of the two arms of the MZI are $l_{1,2}$ and here, we assume that electronic propagation is ballistic and nondispersive within each arm, thus leading to respective times of flights $\tau_{1,2}$. An electronic source (S) is located onto the incoming channel 1 and both incoming channels are at chemical potential μ when the source is off. In this case, the outcoming channels are at the same chemical potential μ.

In full generality, a source generates an excess single electron coherence that propagates through the MZI. The excess Wigner function in the outcoming channel 1 is then given by

$$\Delta W^{(e)}_{1,\mathrm{out}}(t,\omega) = \sum_{j=1,2} \mathcal{M}_{j,j}\, \Delta W^{(e)}_{1,\mathrm{in}}(t-\tau_j,\omega) + 2|\mathcal{M}_{1,2}|\cos(\omega\tau_{12}+\phi)\, \Delta W^{(e)}_{1,\mathrm{in}}(t-\bar{\tau},\omega), \tag{46}$$

where $\tau_{12} = \tau_1 - \tau_2$ and $\bar{\tau} = (\tau_1 + \tau_2)/2$ respectively denote the difference and the average of the two times of flight and $\phi = \mathrm{Arg}(\mathcal{M}_{1,2}) + 2\pi\phi_B$ accounts for the magnetic phase and for eventual phase shifts at the QPC. Note that this translates into the Wigner function formalism the discussion of the ideal MZI interferometer by Haack *et al.*[23] The coefficients $\mathcal{M}_{i,j}$ are associated with the beam splitters and, in the present case,

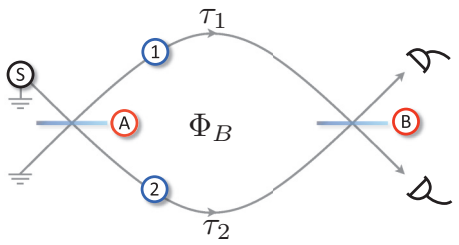

FIG. 8. (Color online) Schematic view of a Mach-Zehnder interferometer: two incoming channels arrive on a beam splitter A and fly along two paths 1 and 2 with respective times of flight τ_1 and τ_2 enclosing a magnetic flux Φ_B and recombine at a beam splitter B. An electronic source (S) is placed on the incoming channel 1.

are given by

$$\mathcal{M}_{1,1} = (1 - T_A)(1 - T_B), \tag{47}$$

$$\mathcal{M}_{2,2} = T_A T_B, \tag{48}$$

$$\mathcal{M}_{1,2} = \sqrt{T_A(1 - T_A)}\sqrt{T_B(1 - T_B)}. \tag{49}$$

In Eq. (46), the first two terms represent the contribution of electrons traveling classically along the two arms of the interferometer whereas the last term represents quantum interference effects associated with propagation along both arms. This quantum term exhibits oscillations in ω taking place over a scale $2\pi/|\tau_{12}|$. Changing the magnetic flux through the MZI interferometer sweeps the phase of these quantum oscillations. These quantum fringes in the Wigner function are indeed characteristic of quantum superpositions. They have been recently observed for Schrödinger cat states in cavity QED[22] and they are now routinely seen in circuit QED experiments.[59–61]

Figure 9 shows the Wigner functions obtained by sending through an ideal MZI an energy-resolved single electron wave packet given by Eq. (41). The two time-shifted wave packets are clearly visible. We have chosen the time of flight difference τ_{12} larger than the duration of each wave packet so that the quantum fringes are clearly visible. In this regime, the two classical components of $\Delta W^{(e)}_{1,\mathrm{out}}(t,\omega)$ are clearly separated from the quantum interference features. Due to the quantum interference contribution, the Wigner function exhibits pronounced regions with negative values thus preventing any quasiclassical interpretation.

Although they could be observed in a full quantum tomography of the single electron coherence,[24] these fringes could also be observed through their impact on the marginal distributions of the Wigner function, that is to say, the average current (24) and the electron distribution function (25).

In order to observe the effect on the average current, the typical scale $2\pi/|\tau_{12}|$ of quantum oscillations in the Wigner function must be comparable or larger than the energy spread of the excess coherence of the source so that these oscillations are not averaged to zero when integrating over ω. This condition expresses that quantum interferences can be observed in the time domain only when the difference of times of flight τ_{12} is comparable or smaller than the coherence time of the source.[44] In the case of a perfectly balanced MZI ($\tau_{12} = 0$), a single peak would be observed in the electron distribution function and in the average current and their heights would be globally modulated by the magnetic flux. In the case of a moderately unbalanced MZI ($\tau_{12} = 2\,\tau_e$) depicted on on Fig. 9(a), the average current shows two overlapping peaks whereas the electron distribution exhibits mainly one peak with some side structure. Changing the magnetic flux by half a quantum decreases the size of the second peak of the average current and also slightly changes the shape and size of the central peak of the electron distribution function.

On the other hand, in the case of a strongly unbalanced MZI ($\tau_{12} = 10\tau_e$), such as the one depicted on Fig. 9(b), interferences cannot be observed using a time-resolved measurement. The average current depicted in Fig. 9(b) (iii) exhibits two peaks that correspond to the two classical

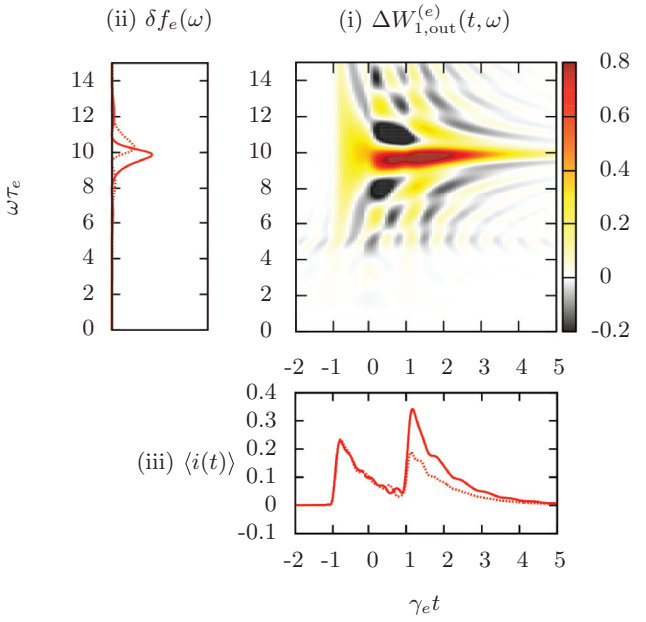

(a) Partly overlapping wave packets: $\tau_{12} = 2\,\tau_e$

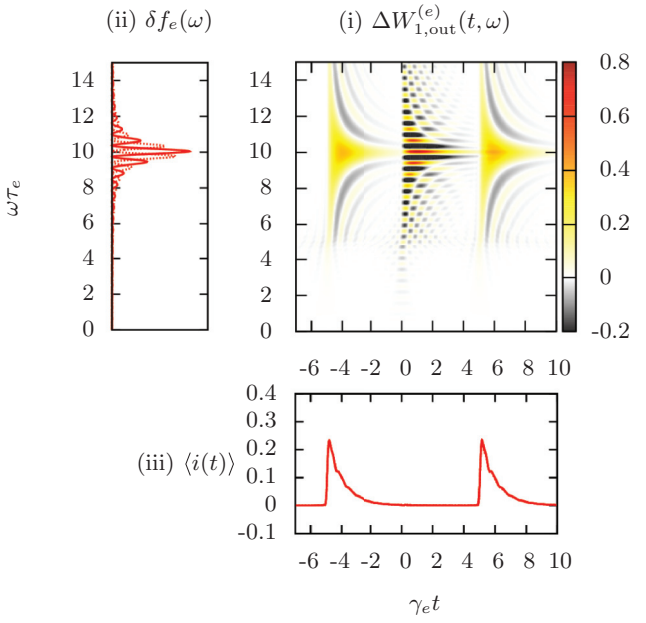

(b) Nonoverlapping wave packets: $\tau_{12} = 10\,\tau_e$

FIG. 9. (Color online) Excess single electron coherence at the output of an ideal Mach-Zehnder interferometer for energy-resolved wave packets (41) emitted at energy $\hbar\omega_e$ and with duration $\tau_e = \gamma_e^{-1}$ such that $\omega_e\tau_e = 10$ and two differences of time of flights τ_{12}: (a) $\tau_{12} = 2\,\tau_e$, (b) $\tau_{12} = 10\,\tau_e$. Each subplot is organized as follows: (i) Density plot of the excess Wigner function $\Delta W^{(e)}_{1,\mathrm{out}}(t,\omega)$ given by Eq. (46) for $\phi = 0$ as a function of t/τ_e and $\omega\tau_e$, (ii) excess electron distribution function $\delta f_e(\omega)$ in the outcoming channel (arbitrary units), (iii) average current $\langle i(t)\rangle$ in units of $-e/\tau_e$. On all graphs, the full line corresponds to $\phi = 0$ whereas the dotted line corresponds to $\phi = \pi$.

contributions to the excess Wigner function. These two peaks do not change when the magnetic flux is varied. In this case, a frequency-resolved detector able to restore the overlap

between electronic wave packets is more appropriate to reveal the interferences. As shown in Fig. 9(b) the quantum fringes of the Wigner function can be observed by measuring the electron distribution function. This is the single electron version of the channeled spectrum observed in optical interferometers using white light.

In practice, observing these effects might be quite challenging due to decoherence within the interferometer itself,[2,62–64] although a proper design of the sample leads to partial protection against decoherence.[65,66] Moreover, observing a channeled spectrum requires an unbalanced interferometer in which $|\tau_{12}|$ is greater than the inverse of the typical energy spreading of the electrons sent into the interferometer. Therefore, the best way to observe a channeled spectrum would be to use a nonequilibrium distribution spreading over a broad energy range such as a double step generated by a QPC[43] or the one generated by an ac sinusoidal voltage. A typical energy range of 100 to 500 μeV corresponds to frequencies from 24 to 120 GHz so that an imbalance of a few μm could be sufficient to observe a channeled spectrum. However, such an experiment would rely on a continuous stream of undistinguishable electrons. In order to observe a channeled spectrum with a single electron source, a larger imbalance is required and excitations that are spread in energy such as Lorentzian pulses[34] with short duration (typically 10 ps) may be appropriate. An alternative approach is to use energy-resolved excitations[8] and change their energies to probe the interferences at the single electron level. But discussing the observability of these effects in a realistic situation would require computing the Wigner distribution function at the output of a Mach-Zehnder interferometer in the presence of interactions, which would go beyond the scope of the present paper.

B. HOM and HBT interferometry

1. *Noise and correlations from coherences*

Two particle interferences are at the heart of the Hanbury Brown and Twiss (HBT) and Hong-Ou-Mandel (HOM) experiments recently demonstrated with single electron excitations emitted by an on-demand single electron source.[37,67] They enable us to imprint information about the single electron coherence into the current noise and correlations issued from an electronic beam splitter of respective reflection and transmission probabilities R and T (see Figs. 10 and 11). This remark underlies the recently proposed single electron tomography protocol aimed at reconstructing an unknown single electron coherence from noise measurements.[24] Predictions have been made for HOM noise signals within the Floquet scattering theory[13,68,69] due to electron and hole coherence[70] and also for the $\nu = 2$ edge channel system with short-range interactions.[71]

The aim of this section is to revisit all these HBT interferometry experiments in terms of the Wigner function. We show that the Wigner function provides a simple and unified view of all these experiments and that it is the quantity of interest for their interpretation.

In the HBT interferometry setup depicted on Fig. 10, the outcoming current correlation between edge channels α and β

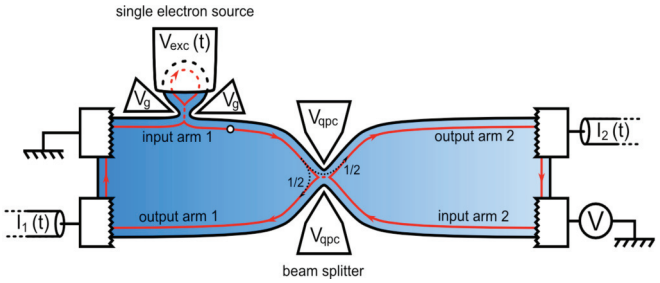

FIG. 10. (Color online) Hanbury Brown and Twiss setup for single electron tomography: This setup is designed to characterize the single electron coherence of an on-demand single electron source present on the incoming branch 1 close to the QPC (here $\mu_1 = 0$) and driven by the voltage $V_{\rm exc}(t)$. A reservoir with a time-dependent chemical potential $\mu_2(t) = -eV(t) = \mu_2 - eV_{\rm ac}(t)$ is connected to the incoming branch 2. One measures the low-frequency correlation $S_{12}^{\rm exp}$ of the outcoming current I_1 and I_2.

is defined as

$$S^{\rm out}_{\alpha\beta}(t,t') = \langle i^{\rm out}_\alpha(t)\, i^{\rm out}_\beta(t')\rangle - \langle i^{\rm out}_\alpha(t)\rangle\langle i^{\rm out}_\beta(t')\rangle. \tag{50}$$

The final expressions for outcoming current correlations are[24]

$$S^{\rm out}_{11} = R^2 S^{\rm in}_{11} + T^2 S^{\rm in}_{22} + RT\,\mathcal{Q}, \tag{51a}$$

$$S^{\rm out}_{22} = T^2 S^{\rm in}_{11} + R^2 S^{\rm in}_{22} + RT\,\mathcal{Q}, \tag{51b}$$

$$S^{\rm out}_{12} = S^{\rm out}_{21} = RT\left(S^{\rm in}_{11} + S^{\rm in}_{22} - \mathcal{Q}\right), \tag{51c}$$

where for simplicity we have omitted the (t,t') arguments. These outcoming correlations involve the incoming ones $S^{\rm in}_{\alpha\beta}(t,t')$ and a contribution $\mathcal{Q}(t,t')$ coming from two-particle interferences. This contribution $\mathcal{Q}(t,t')$ involves the incoming single particle coherences right upstream the QPC:

$$\mathcal{Q}(t,t') = (ev_F)^2\left(\mathcal{G}^{(e)}_1\mathcal{G}^{(h)}_2 + \mathcal{G}^{(e)}_2\mathcal{G}^{(h)}_1\right)(t',t), \tag{52}$$

where, for HBT interferometry, $\mathcal{G}^{(e)}_2$ and $\mathcal{G}^{(h)}_2$ are the electron and hole coherences emitted by a reservoir at chemical potential μ_2 and electronic temperature $T_{\rm el}$.

As discussed in Sec. II A, electron quantum optics differs from photon quantum optics on the nature of the vacuum. Even

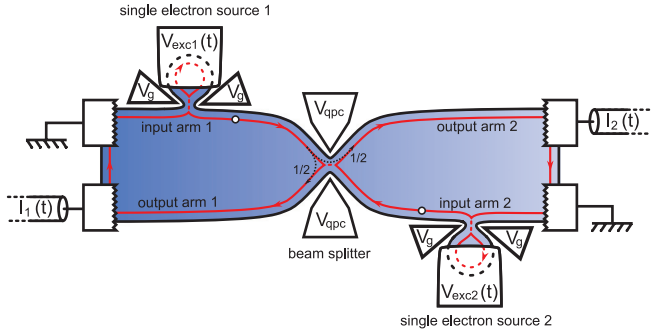

FIG. 11. (Color online) Sketch of the usual Hong-Ou-Mandel experiment (Ref. 37): On demand single electron sources are present on each incoming branch and are driven by time-shifted voltages: $V_{{\rm exc},2}(t) = V_{{\rm exc},1}(t - \Delta t)$. One measures the low-frequency correlation $S_{12}^{\rm exp}$ of the outcoming current I_1 and I_2.

when sources are switched off, a nonvanishing single electron coherence is present and, at nonzero temperature, leads to a nonzero current noise. We shall thus consider situations in which no source is switched on (off/off), one of the two is switched on (cases on/off and off/on), and both are switched on (on/on). Denoting by ΔX the difference between X in the situation under consideration and X when the two sources are off, we obtain

$$\Delta S_{11}^{\mathrm{on/off}} = R^2 \Delta S_{11}^{\mathrm{in}} + RT(\Delta\mathcal{Q})_{\mathrm{on/off}}, \tag{53a}$$

$$\Delta S_{11}^{\mathrm{off/on}} = T^2 \Delta S_{22}^{\mathrm{in}} + RT(\Delta\mathcal{Q})_{\mathrm{off/on}}, \tag{53b}$$

where the HBT excess contribution in Eq. (53a) is given by

$$(\Delta\mathcal{Q})_{\mathrm{on/off}}(t,t') = (ev_F)^2\big(\Delta\mathcal{G}_1^{(e)}\mathcal{G}_2^{(h)} + \Delta\mathcal{G}_1^{(h)}\mathcal{G}_2^{(e)}\big)(t',t), \tag{54}$$

with a similar expression for $(\Delta\mathcal{Q})_{\mathrm{off/on}}(t,t')$. These expressions are relevant when one of the incoming channel is populated by an equilibrium distribution. Since an equilibrium state is the analog of the vacuum for photons in the electron quantum optics channel; such a situation is analogous to the historical table-top HBT experiment.[31] It has been recently demonstrated with an on-demand single electron source.[67]

In the case of an HOM experiment (see Fig. 11), the two sources are switched on. In this case, the excess outcoming noise $\Delta S_{11}^{\mathrm{on/on}}$ is the sum of the excess HBT noises and of an HOM contribution corresponding to two-particle interferences between excitations emitted by both sources:

$$\Delta S_{11}^{\mathrm{on/on}} = \Delta S_{11}^{\mathrm{on/off}} + \Delta S_{11}^{\mathrm{off/on}} + RT(\Delta\mathcal{Q})_{\mathrm{HOM}}. \tag{55}$$

This HOM contribution (with respect to the situation where the two sources are switched off) is defined as

$$(\Delta\mathcal{Q})_{\mathrm{HOM}}(t,t') = (ev_F)^2\big(\Delta\mathcal{G}_1^{(e)}\Delta\mathcal{G}_2^{(h)} + (1\leftrightarrow 2)\big)(t',t). \tag{56}$$

In electronic transport, one can only access the time average of current correlations at a given frequency Ω:

$$S_{\alpha\beta}^{\mathrm{exp}}(\Omega) = \int \overline{S_{\alpha\beta}^{\mathrm{out}}(\bar{t}+\tau/2,\bar{t}-\tau/2)}^{\bar{t}}\, e^{i\Omega\tau} d\tau. \tag{57}$$

Although the experiments are often performed at low frequency ($\Omega \simeq 0$), recent progress in finite-frequency noise measurements[18] motivates considering the case of finite-frequency noise. As a consequence, the HBT and HOM excess contributions to the experimental signals are given by overlaps in time of two excess coherences. Thanks to Plancherel's theorem, they can also be expressed as overlaps of the corresponding Wigner functions. As we shall see, this makes the physical interpretation of the HBT and HOM two-particle interferometry experiments extremely transparent.

2. A Wigner view on the HBT and HOM experiments

To begin with, let us first consider the HBT excess contribution given by Eq. (54). Rewriting excess hole coherences in terms of electronic coherences and performing the time averaging and Fourier transform as in Eq. (57) leads to the excess HBT contribution of the outcoming noise under the form

$$(\Delta\mathcal{Q})_{\mathrm{on/off}}(\Omega) = -e\langle i_1\rangle - e^2\int \delta f_1(\omega)\, g_2(\omega,\Omega)\frac{d\omega}{2\pi}, \tag{58}$$

where $\langle i_1\rangle$ denotes the average dc current of source 1, $\delta f_1(\omega) = \overline{\Delta W_1^{(e)}(t,\omega)}^{t}$ is the excess electron distribution function in the incoming channel 1, and

$$g_2(\omega,\Omega) = f_2(\omega-\Omega) + f_2(\omega+\Omega) \tag{59}$$

is a double step going from zero for $\omega \gg |\Omega|$ to 2 for $\omega \ll -|\Omega|$ through an intermediate plateau at 1 for $|\omega| \lesssim |\Omega|$. The steps are thermally broadened over an energy scale $k_B T_{\mathrm{el}}$. Let us first remark that the result depends on the excess electron distribution function $\delta f_1(\omega)$ which is precisely the time average of the excess electronic Wigner function in the incoming channel 1. This is expected since we are measuring a time-averaged quantity and the incoming channel 2 is populated with a stationary (equilibrium) state.

The first contribution on the right-hand side of Eq. (58) corresponds to classical (Poissonian) partitioning of electrons and hole excitations sent in the incoming channel 1. Since this noise has a white spectrum, the corresponding term is independent from Ω.

The second term on the right-hand side of Eq. (58) is an even function of Ω. Its minus sign arises from the fermionic statistics of electrons and expresses antibunching. In fact, Eqs. (51) and (52) are also valid for bosons but the relation between particle and antiparticle coherences would lead to a plus sign in the case of bosons in Eq. (58). In an experiment with bosons, $g_2(\omega,\Omega)$ would involve the bosonic occupation number in a stationary reference beam arriving from input arm 2. To understand the frequency dependence, we rewrite the average dc current in terms of the excess electron distribution function. Equation (58) then becomes

$$(\Delta\mathcal{Q})_{\mathrm{on/off}}(\Omega) = e^2\int \delta f_1(\omega)\,[1-g_2(\omega,\Omega)]\,\frac{d\omega}{2\pi}. \tag{60}$$

This shows that at zero temperature, the excess HBT contribution is given by the sum of electronic excitations and of hole excitations whose energies exceed $\hbar|\Omega|$. This expression generalizes the formula known for the outcoming current noise at zero frequency.[67]

Let us now discuss the case of an HOM experiment. The same line of reasoning shows that the HOM contribution given by Eq. (56) is the overlap of the excess Wigner functions arriving from the two incoming channels:

$$(\Delta\mathcal{Q})_{\mathrm{HOM}}(\Omega) = -e^2\int \Big[\overline{\Delta W_1^{(e)}(t,\omega)\,\Delta W_2^{(e)}(t,\omega+\Omega)}^{t} + \overline{\Delta W_2^{(e)}(t,\omega)\,\Delta W_1^{(e)}(t,\omega+\Omega)}^{t}\Big]\frac{d\omega}{2\pi}. \tag{61}$$

This simple expression immediately suggests what happens physically: this term will contribute only when the excitations emitted by the two sources overlap up to the frequency shift at which outcoming current noise or correlations are measured. Consequently, the noise and correlation in the HOM experiment contains interesting information about the single electron coherences injected in the HBT interferometer. Whereas the usual HOM experiment gives access to the overlap

of the excess Wigner functions of the two sources modulo an experimentally controlled time shift, finite-frequency measurements enable us to probe a shift in energy. As a consequence, such measurements, although notably difficult,[18] could be used to obtain qualitative information on relaxation mechanisms.

Finally, in the case of two ideal single electron sources, each one emitting a single electron wave packet per period characterized by its wave function $\varphi_{1,2}$, the HOM contribution at low frequency reduces to[38]

$$(\Delta\mathcal{Q})_{\mathrm{on/on}}(\Omega=0) = -2e^2 f\,|\langle\varphi_1|\varphi_2\rangle|^2. \qquad (62)$$

However, note that this interpretation of the HOM contribution as a wave packet overlap is specific to ideal sources emitting well-defined and coherent single electron wave packets. But this is not true in general:[13,46] in full generality, the proper way to understand the outcome of an HOM experiment is in terms of overlaps of single electron coherences even in the case where many electron/hole pairs are present. The Wigner representation provides a transparent way to visualize what contributes to the experimental HOM signals.

3. *Single electron tomography revisited*

Expressions (58) and (61) enable us to understand the recently proposed single electron tomography protocol[24] in a very simple way. As in the case of optical homodyne tomography,[72,73] the key is to find a controlled source which, by varying its parameters, will enable us to reconstruct the single electron coherence emitted by the source to be characterized or, equivalently, $\Delta W_1^{(e)}(t,\omega)$.

A natural source that spans the whole space of single electron states is an equilibrium reservoir: depending on its chemical potential, some states will be filled and others will be empty. Its Wigner function is constant in time and equal to the equilibrium Fermi distribution of the reservoir. Let us assume zero temperature for simplicity: by increasing the chemical potential, the second term on the right-hand side of Eq. (58) will include an additional small slice in frequency of the unknown Wigner function. Equation (58) expresses that the change in current noise when increasing the chemical potential from μ_2 to $\mu_2 + d\mu_2$ is proportional to the population of single electron states within the incoming channel 1 whose energies are between μ_2 and $\mu_2 + d\mu_2$. If such a state is populated, the incoming electrons from both sides antibunch and the noise does not change. If such a state is empty, the electron emitted by the battery into this interval will be partitioned at the beam splitter adding a contribution to the noise. This is the idea of shot noise spectroscopy originally discussed in the context of photon-assisted shot noise[74,75] and more recently in the context of electron quantum optics.[24,76]

To capture the time dependance of the unknown excess Wigner function $\Delta W_1^{(e)}(t,\omega)$, a time-dependent source is required. As seen in Sec. III A2, in the limit of small drive ($eV_0 \ll hf$), the Wigner distribution issued by a reservoir driven by a small sinusoidal voltage $V_d(t) = V_0\cos(2\pi nft + \phi_0)$ is given at first order by

$$\frac{\partial\Delta W_2^{(e)}(t,\omega)}{\partial(eV_0/hf)} = -2\cos(2\pi nft+\phi_0)F_{\mu,T_{\mathrm{el}}}(\omega), \qquad (63)$$

where $F_{\mu,T_{\mathrm{el}}}(\omega)$ is the convolution of the characteristic function of the interval $[\mu/\hbar-\pi f,\mu/\hbar+\pi f]$ with $-[4k_BT_{\mathrm{el}}\cosh^2(\hbar\omega/2k_BT_{\mathrm{el}})]^{-1}$. Equation (63) combined with Eq. (61) at zero frequency shows that in the Wigner distribution point of view, the response of the low-frequency noise to a small dc drive applied on the incoming channel 2 contains the information about the Fourier transform in time of the excess Wigner distribution of the source to be characterized. In practice, the finite electronic temperature introduces a blurring of the Wigner function along the energy direction over a scale k_BT_{el}.

Approaching single electron tomography from the Wigner function point of view immediately raises the question of alternative tomography protocols based on other reference signals. This question is strongly motivated by the problem of efficiency: single electron tomography based on HOM-like experiments relies on ultrahigh-sensitivity current noise measurements which can be quite costly in terms of acquisition time.[37]

Our generic tomography protocol[24] reconstructs the unknown excess Wigner function $\Delta W_1^{(e)}(t,\omega)$ by extracting from noise measurements its t dependence at fixed ω as a Fourier series. The various examples discussed in the present paper suggest that getting an accurate view of these coherences may require heavy sampling in ω as well as in the number of harmonics. It would thus be highly desirable to design alternative protocols based on a different controlled source so that a much lighter sampling is required to obtain an accurate picture of the Wigner function. This problem is reminiscent of the problematic of compressive sensing[33,77] but here we deal with single electron coherence which is a "quantum signal." The HOM experiment automatically generates the overlap between two such "quantum signals." The practical problem is then to find which controlled source could lead to an accurate approximation of the unknown Wigner function through a minimal number of noise measurements in an HOM experiment.

This problem may lead to some interesting theoretical developments but in practice, very few well controlled sources are available. The ac and dc drive lead to our generic tomography protocol. The energy-resolved excitations discussed in Sec. III B1 cannot be considered as controlled due to decoherence between the mesoscopic capacitor and the QPC. Indeed, characterizing decoherence effects on single electron excitations is precisely one of the main motivation for single electron tomography. On the contrary, voltage pulses can be considered as controlled to some extent: high-frequency current measurements[16] can be used to control the shape of the pulse arriving onto the QPC, although in a limited bandwidth. Moreover, noise measurement can help characterizing purely electronic pulses.[13,34] Specific voltage pulses may thus provide interesting families of functions to reconstruct single electron coherence at minimal cost in some cases. However, finding out the appropriate family of excitations requires an *a priori* knowledge of the signal to be measured. Forthcoming and foreseeable experiments will certainly involve decoherence effects. Therefore, designing alternative tomography protocols based on HOM experiments requiring less measurements calls for an in depth modeling of decoherence in the Wigner function formalism. This would go beyond the scope of the

present paper but is of clear interest from this signal-processing perspective.

V. CONCLUSION

In this paper, we have introduced the time-frequency representation of the single electron coherence in quantum Hall edge channels generalizing the quasiprobability distribution function introduced in quantum mechanics[19] and commonly used in quantum optics. We have shown that this real valued function of time and frequency provides a very convenient way to image single electron coherence in a quantum conductor. It gives access to both the energy content and real time development of excitations emitted by electron sources, shedding new light on electron coherence and discussing it in a signal-processing language. It also provides a natural framework to deal with the quantum nature of electron excitations, in which quantum interferences effects have a clear signature as pronounced nonclassical regions where the Wigner function violates the bounds required by the Pauli principle and to interpret it as a probability distribution. Along the same lines, it leads straightforwardly to the emergent semiclassical picture of the quasiparticle dynamics.

Moreover, the celebrated HBT and HOM interferometry experiments have a very simple interpretation in terms of overlaps of Wigner functions. Consequently, Wigner function computations are directly useful to interpret the results of these experiments at both qualitative and quantitative levels. In fact, our main message is that the Wigner function is a very relevant representation of single electron coherence because it provides a simple and unified view of many single and two particle interference effects that have been experimentally demonstrated in electron quantum optics and quantum nanoelectronics over the last fifteen years.[1,2,6,37,67]

Experimentally, measuring single electron coherence or equivalently the Wigner function is an important but difficult challenge for electron quantum optics. However, as discussed in the present paper, we think that a variety of techniques is now available to recover information on the Wigner function ranging from amplitude interferometry[23,44] to the HOM experiment and its many possible variants among which is the recently proposed single electron tomography protocol.[24]

To conclude, an important and still open question in electron quantum optics is to compute the Wigner function taking into account the effects of interactions experienced by the excitations emitted by a single electron source. In the case of pure single electron excitations, the bosonization technique already used to discuss the problem of quasiparticle relaxation in quantum Hall edge channels[39] can be adapted. This leads to a complete unraveling of decoherence scenarios of single electron excitations in quantum Hall edge channels which will be discussed in a future publication.

ACKNOWLEDGMENTS

We thank B. Roussel from ENS Lyon and Q. Lavigne from Telecom St. Etienne for their valuable help in data visualization. We also thank J. M. Berroir and B. Plaçais from LPA as well as Th. Jonckheere, Th. Martin, J. Rech, and C. Wahl from CPT Marseille for useful discussions. We thank G. Haack for useful comments. We finally thank P. Borgnat from ENS Lyon for discussions about time/frequency representation in signal processing and compressed sensing. This work is supported by the ANR grant "1shot" (ANR-2010-BLANC-0412). E.B. acknowledges funding from the Alexander von Humboldt Foundation.

APPENDIX A: PROPERTIES OF SINGLE ELECTRON COHERENCE

1. Basic properties

As in photon quantum optics, first-order coherences satisfy the Hermiticity property:

$$\mathcal{G}^{(e)}_{\rho}(x,t;y,t')^* = \mathcal{G}^{(e)}_{\rho}(y,t';x,t), \tag{A1a}$$

$$\mathcal{G}^{(h)}_{\rho}(x,t;y,t')^* = \mathcal{G}^{(h)}_{\rho}(y,t';x,t). \tag{A1b}$$

In a region of free chiral ballistic propagation at velocity v_F, the single electron coherence obeys

$$\mathcal{G}^{(e)}_{\rho}(x+v_F\tau,t+\tau;x'+v_F\tau,t'+\tau) = \mathcal{G}^{(e)}_{\rho}(x,t;x',t'). \tag{A2}$$

When considering coherences at a position x where propagation can be assumed to be free, Eq. (3) translates into a relation between electron and hole coherences in the time domain:

$$\mathcal{G}^{(e)}_{\rho,x}(t,t') = v_F^{-1}\delta(t-t') - \mathcal{G}^{(h)}_{\rho,x}(t',t). \tag{A3}$$

Taking the Fourier transform of this equation with respect to $t-t'$ immediately leads to the relation between electron and hole Wigner functions (21).

In order to connect single electron coherence to the fermionic occupation number, we decompose

$$\psi(x,t) = \int e^{-i\omega t} c(\omega)\,\frac{d\omega}{\sqrt{2\pi v_F}}, \tag{A4}$$

where $c(\omega)$ and $c^\dagger(\omega)$ respectively create and destroy an electron at energy $\hbar\omega$ with respect to the reference Fermi energy. These operators satisfy the canonical anticommutation relations: $\{c(\omega),c(\omega')\} = 0$ and $\{c(\omega),c^\dagger(\omega')\} = \delta(\omega-\omega')$.

2. Cauchy-Schwarz inequalities

Finally, the single electron coherence satisfies a Cauchy-Schwarz inequality associated with the Hermitian product on the operator space: $(A|B) = \mathrm{Tr}(B\rho A^\dagger)$. Due to the nonzero coherence of the Fermi sea, this inequality is most useful in the frequency domain at zero temperature. Using $A = c(\omega_-)$, $B = c(\omega_+)$, and Eq. (17), we write the Cauchy-Schwarz inequality:

$$\left|\widetilde{\mathcal{G}}^{(e)}_{\rho,x}(\omega_+,\omega_-)\right|^2 \leqslant \widetilde{\mathcal{G}}^{(e)}_{\rho,x}(\omega_+,\omega_+)\,\widetilde{\mathcal{G}}^{(e)}_{\rho,x}(\omega_-,\omega_-). \tag{A5}$$

Decomposing $\widetilde{\mathcal{G}}^{(e)}_{\rho,x}$ into a Fermi sea contribution at chemical potential $\mu = 0$ and an excess contribution which we assume to be regular

$$\widetilde{\mathcal{G}}^{(e)}_{\rho,x}(\omega_+,\omega_-) = \frac{2\pi}{v_F}\delta(\omega_+-\omega_-)\Theta(-\omega_+) + \Delta\widetilde{\mathcal{G}}^{(e)}_{\rho,x}(\omega_+,\omega_-) \tag{A6}$$

and taking ω_+ and ω_- positive shows that the Fermi sea contribution vanishes and leads to the following inequality

satisfied over the (e) quadrant (see Fig. 1):

$$\left|\Delta\widetilde{\mathcal{G}}^{(e)}_{\rho,x}(\omega_+,\omega_-)\right|^2 \leqslant \Delta\widetilde{\mathcal{G}}^{(e)}_{\rho,x}(\omega_+,\omega_+)\,\Delta\widetilde{\mathcal{G}}^{(e)}_{\rho,x}(\omega_-,\omega_-). \quad \text{(A7)}$$

Considering the hole coherence and $\omega_\pm < 0$, the same line of reasoning shows that the inequality (A7) is also true in the (h) quadrant.

Finally, let us consider $\omega_- < 0$ and $\omega_+ > 0$ and assume that the excess single electron coherence does not contribute to the electron occupation below the Fermi level $\Delta\widetilde{\mathcal{G}}^{(e)}_{\rho,x}(\omega_-,\omega_-) = 0$. Then, the general inequality (A5) implies that $\Delta\widetilde{\mathcal{G}}^{(e)}_{\rho,x}(\omega_+,\omega_-)$ also vanishes: there are no electron/hole coherences. The same reasoning can be done on hole coherences and shows that there are no electron/hole coherences if the source does not contribute to the excess occupation number of electrons. Finally, the inequality (A7) also shows that if a source does not contribute to the excess hole (resp. electron) occupation number, it has vanishing coherence in the (h) quadrant [resp. (e) quadrant]. This proves that, at zero temperature, as soon as a source does not lead to an excess of electrons (resp. holes), it only contributes to the excess coherence in the (h) [resp. (e)] quadrant. In other words, it only generates hole (resp. electronic) excitations.

APPENDIX B: ENERGY-RESOLVED ELECTRONIC WAVE PACKET

It is possible to obtain an analytic formula for the truncated Lorentzian wave packet (41) in the time domain. Depending on the sign of t, we build a closed contour that contains the positive real axis and either the positive or negative imaginary axis. The integral over the imaginary half axis can then be expressed in terms of the exponential integral function[48] $\mathrm{Ei}(x)$. This leads to

$$\varphi_e(t) = \frac{-i\mathcal{N}_\mathrm{e}}{\sqrt{v_F\tau_\mathrm{e}}}\, e^{-\gamma_\mathrm{e}t/2 - i\omega_\mathrm{e}t}\left(\Theta(t) - \frac{i}{2\pi}\mathrm{Ei}\left[\left(\frac{\gamma_\mathrm{e}}{2} + i\omega_\mathrm{e}\right)t\right]\right), \quad \text{(B1)}$$

where $\mathcal{N}_\mathrm{e} = [\frac{1}{2} + \frac{1}{\pi}\arctan(\frac{2\omega_\mathrm{e}}{\gamma_\mathrm{e}})]^{-1/2}$ is the normalization factor. The exponential integral part is responsible for the nonvanishing of the wave packet for $t < 0$ and for the oscillations of its envelope at $t > 0$. These features can be observed on the numerical evaluation of excess single electron coherence $\varphi_e(\bar{t} + \tau/2)\varphi_e^*(\bar{t} - \tau/2)$ depicted in Fig. 5(c) as well as on the current density $v_F|\varphi_e(t)|^2$ computed from the Wigner function [see panels (iii) in Fig. 9]. Note that Eq. (B1) predicts a $\log(t/\tau_\mathrm{e})$ singularity of $\varphi_e(t)$ at $t = 0$ which is not visible in the numerics due to the UV cutoff in numerical integration.

[1] Y. Ji, Y. Chung, D. Sprinzak, M. Heiblum, D. Mahalu, and H. Shtrikman, Nature (London) **422**, 415 (2003).
[2] P. Roulleau, F. Portier, D. C. Glattli, P. Roche, A. Cavanna, G. Faini, U. Gennser, and D. Mailly, Phys. Rev. B **76**, 161309 (2007).
[3] W. Oliver, J. Kim, R. Liu, and Y. Yamamoto, Science **284**, 299 (1999).
[4] M. Henny, S. Oberholzer, C. Strunk, T. Heinzel, K. Ensslin, M. Holland, and C. Schönenberger, Science **284**, 296 (1999).
[5] P. Samuelsson, E. V. Sukhorukov, and M. Büttiker, Phys. Rev. Lett. **92**, 026805 (2004).
[6] I. Neder, N. Ofek, Y. Chung, M. Heiblum, D. Mahalu, and V. Umansky, Nature (London) **448**, 333 (2007).
[7] F.-J. Ahlers, O. Kieler, B. Sagol, K. Pierz, and U. Siegner, J. Appl. Phys. **100**, 093702 (2006).
[8] G. Fève, A. Mahé, J.-M. Berroir, T. Kontos, B. Plaçais, D. C. Glattli, A. Cavanna, B. Etienne, and Y. Jin, Science **316**, 1169 (2007).
[9] M. Blumenthal, B. Kaestner, L. Li, S. Giblin, T. Janssen, M. Pepper, D. Anderson, G. Jones, and D. Ritchie, Nat. Phys. **3**, 343 (2007).
[10] C. Leicht, P. Mirovsky, B. Kaestner, F. Hols, V. Kashcheyevs, E. Kurganova, U. Zeitler, T. Weimann, K. Pierz, and H. Schumacher, Semicond. Sci. Technol. **26**, 055010 (2011).
[11] F. Battista and P. Samuelsson, Phys. Rev. B **83**, 125324 (2011).
[12] S. Hermelin, S. Takada, M. Yamamoto, S. Tarucha, A. Wieck, L. Saminadayar, C. Bäuerle, and T. Meunier, Nature (London) **477**, 435 (2011).
[13] J. Dubois, T. Jullien, C. Grenier, P. Degiovanni, P. Roulleau, and D. C. Glattli, Phys. Rev. B **88**, 085301 (2013).
[14] C. Grenier, R. Hervé, G. Fève, and P. Degiovanni, Mod. Phys. Lett. B **25**, 1053 (2011).
[15] J. Gabelli, G. Fève, J.-M. Berroir, B. Plaçais, A. Cavanna, B. Etienne, Y. Jin, and D. C. Glattli, Science **313**, 499 (2006).
[16] E. Bocquillon, V. Freulon, J.-M. Berroir, P. Degiovanni, B. Plaçais, A. Cavanna, Y. Jin, and G. Fève, Nat. Commun. **4**, 1839 (2013).
[17] A. Mahé, F. D. Parmentier, E. Bocquillon, J.-M. Berroir, D. C. Glattli, T. Kontos, B. Plaçais, G. Fève, A. Cavanna, and Y. Jin, Phys. Rev. B **82**, 201309 (2010).
[18] F. D. Parmentier, A. Mahé, A. Denis, J.-M. Berroir, D. C. Glattli, B. Plaçais, and G. Fève, Rev. Sci. Instrum. **82**, 013904 (2011).
[19] E. Wigner, Phys. Rev. **40**, 749 (1932).
[20] J. Ville, Câbles et Transmission **2**, 61 (1948).
[21] D. Walls and G. Milburn, *Quantum Optics* (Springer-Verlag, Berlin, 1994).
[22] S. Deléglise, I. Dotsenko, C. Sayrin, J. Bernu, M. Brune, J.-M. Raimond, and S. Haroche, Nature (London) **455**, 510 (2008).
[23] G. Haack, M. Moskalets, and M. Büttiker, Phys. Rev. B **87**, 201302 (2013).
[24] C. Grenier, R. Hervé, E. Bocquillon, F. D. Parmentier, B. Plaçais, J.-M. Berroir, G. Fève, and P. Degiovanni, New J. Phys. **13**, 093007 (2011).
[25] C. Jacoboni and P. Bordone, Rep. Prog. Phys. **67**, 1033 (2004).
[26] P. Bordone, M. Pascoli, R. Brunetti, A. Bertoni, C. Jacoboni, and A. Abramo, Phys. Rev. B **59**, 3060 (1999).
[27] W. R. Frensley, Phys. Rev. B **36**, 1570 (1987).
[28] N. C. Kluksdahl, A. M. Kriman, D. K. Ferry, and C. Ringhofer, Phys. Rev. B **39**, 7720 (1989).
[29] L. G. Lutterbach and L. Davidovich, Phys. Rev. Lett. **78**, 2547 (1997).
[30] F. de Melo, L. Aolita, F. Toscano, and L. Davidovich, Phys. Rev. A **73**, 030303(R) (2006).
[31] R. Hanbury Brown and R. Twiss, Nature (London) **177**, 27 (1956).
[32] C. K. Hong, Z. Y. Ou, and L. Mandel, Phys. Rev. Lett. **59**, 2044 (1987).
[33] Y. C. Eldar and G. Kutyniok, *Compressed Sensing: Theory and Applications* (Cambridge University Press, New York, 2012).

[34]J. Dubois, T. Jullien, F. Portier, P. Roche, A. Cavanna, Y. Jin, W. Wegscheider, P. Roulleau, and D. C. Glattli, Nature (London) **502**, 659 (2013); see also J. Dubois, Ph.D. thesis, Université de Paris-Sud, 2012.
[35]D. S. Golubev and A. D. Zaikin, Phys. Rev. B **59**, 9195 (1999).
[36]K. E. Cahill and R. J. Glauber, Phys. Rev. A **59**, 1538 (1999).
[37]E. Bocquillon, V. Freulon, J.-M. Berroir, P. Degiovanni, B. Plaçais, A. Cavanna, Y. Jin, and G. Fève, Science **339**, 1054 (2013).
[38]G. Fève, P. Degiovanni, and T. Jolicoeur, Phys. Rev. B **77**, 035308 (2008).
[39]P. Degiovanni, C. Grenier, and G. Fève, Phys. Rev. B **80**, 241307(R) (2009).
[40]G. Haack, Ph.D. thesis, Université de Genève, 2012.
[41]R. Glauber, Phys. Rev. Lett. **10**, 84 (1963).
[42]R. Glauber, Phys. Rev. **130**, 2529 (1963).
[43]C. Altimiras, H. le Sueur, U. Gennser, A. Cavanna, D. Mailly, and F. Pierre, Nat. Phys. **6**, 34 (2010).
[44]G. Haack, M. Moskalets, J. Splettstoesser, and M. Büttiker, Phys. Rev. B **84**, 081303 (2011).
[45]P. Bertet, A. Auffèves, P. Maioli, S. Osnaghi, T. Meunier, M. Brune, J. M. Raimond, and S. Haroche, Phys. Rev. Lett. **89**, 200402 (2002).
[46]C. Grenier, J. Dubois, T. Jullien, P. Roulleau, D. C. Glattli, and P. Degiovanni, Phys. Rev. B **88**, 085302 (2013).
[47]G. B. Lesovik and L. S. Levitov, Phys. Rev. Lett. **72**, 538 (1994).
[48]I. Gradshteyn and I. Ryzhik, *Table of Integrals, Series, and Products*, 5th ed. (Academic Press, Inc., Boston, 1994).
[49]M. Moskalets and M. Büttiker, Phys. Rev. B **66**, 205320 (2002).
[50]M. Moskalets, P. Samuelsson, and M. Büttiker, Phys. Rev. Lett. **100**, 086601 (2008).
[51]M. Moskalets and M. Büttiker, Phys. Rev. B **75**, 035315 (2007).
[52]M. Moskalets, Phys. Rev. B **88**, 035433 (2013).
[53]F. D. Parmentier, E. Bocquillon, J.-M. Berroir, D. C. Glattli, B. Plaçais, G. Fève, M. Albert, C. Flindt, and M. Büttiker, Phys. Rev. B **85**, 165438 (2012).
[54]A. Mahé, F. D. Parmentier, G. Fève, J.-M. Berroir, T. Kontos, A. Cavanna, B. Etienne, Y. Jin, D. C. Glattli, and B. Plaçais, J. Low Temp. Phys. **153**, 339 (2008).
[55]S. E. Nigg and M. Büttiker, Phys. Rev. B **77**, 085312 (2008).
[56]L. Levitov, H. Lee, and G. Lesovik, J. Math. Phys. **37**, 4845 (1996).
[57]D. A. Ivanov, H. W. Lee, and L. S. Levitov, Phys. Rev. B **56**, 6839 (1997).
[58]J. Gabelli and B. Reulet, Phys. Rev. B **87**, 075403 (2013).
[59]H. Wang, M. Hofheinz, M. Ansmann, R. C. Bialczak, E. Lucero, M. Neeley, A. D. O'Connell, D. Sank, M. Weides, J. Wenner *et al.*, Phys. Rev. Lett. **103**, 200404 (2009).
[60]M. Hofheinz, H. Wang, M. Ansmann, R. Biazlczak, E. Lucero, M. Neeley, A. O'Connell, D. Sank, J. Wenner, J. Martinis *et al.*, Nature (London) **459**, 546 (2009).
[61]Y. Shalibo, R. Resh, O. Fogel, D. Shwa, R. Bialczak, J. M. Martinis, and N. Katz, Phys. Rev. Lett. **110**, 100404 (2013).
[62]P. Roulleau, F. Portier, P. Roche, A. Cavanna, G. Faini, U. Gennser, and D. Mailly, Phys. Rev. Lett. **101**, 186803 (2008).
[63]P. Roulleau, F. Portier, D. C. Glattli, P. Roche, A. Cavanna, G. Faini, U. Gennser, and D. Mailly, Phys. Rev. Lett. **100**, 126802 (2008).
[64]I. Neder, F. Marquardt, M. Heiblum, D. Mahalu, and V. Umansky, Nat. Phys. **3**, 534 (2007).
[65]C. Altimiras, H. le Sueur, U. Gennser, A. Cavanna, D. Mailly, and F. Pierre, Phys. Rev. Lett. **105**, 226804 (2010).
[66]P.-A. Huynh, F. Portier, H. le Sueur, G. Faini, U. Gennser, D. Mailly, F. Pierre, W. Wegscheider, and P. Roche, Phys. Rev. Lett. **108**, 256802 (2012).
[67]E. Bocquillon, F. D. Parmentier, C. Grenier, J.-M. Berroir, P. Degiovanni, D. C. Glattli, B. Plaçais, A. Cavanna, Y. Jin, and G. Fève, Phys. Rev. Lett. **108**, 196803 (2012).
[68]S. Ol'khovskaya, J. Splettstoesser, M. Moskalets, and M. Büttiker, Phys. Rev. Lett. **101**, 166802 (2008).
[69]M. Moskalets, G. Haack, and M. Büttiker, Phys. Rev. B **87**, 125429 (2013).
[70]T. Jonckheere, J. Rech, C. Wahl, and T. Martin, Phys. Rev. B **86**, 125425 (2012).
[71]C. Wahl, J. Rech, T. Jonckheere, and T. Martin, arXiv:1307.5257.
[72]D. T. Smithey, M. Beck, M. G. Raymer, and A. Faridani, Phys. Rev. Lett. **70**, 1244 (1993).
[73]A. I. Lvovsky and M. G. Raymer, Rev. Mod. Phys. **81**, 299 (2009).
[74]A. Kozhevnikov, Ph.D. thesis, Yale University, 2001.
[75]A.V. Shytov, Phys. Rev. B **71**, 085301 (2005).
[76]M. Moskalets and M. Büttiker, Phys. Rev. B **83**, 035316 (2011).
[77]E. Candès, in *Proceedings of the International Congress of Mathematicians* (European Mathematical Society, Zurich, 2006), Vol. III.
[78]Working with equal time coherences, we drop the time dependence for simplicity. Note that in the present case, $g^{(1)}(x,l)$ is well defined only when the product $\Delta\mathcal{G}^{(e)}_{\rho}(x+l/2,x+l/2)\,\Delta\mathcal{G}^{(e)}_{\rho}(x-l/2,x-l/2)$ is positive. But for a source emitting only electrons, this is always the case.